Article

Cell

An Activity Switch in Human Telomerase Based on RNA Conformation and Shaped by TCAB1

Graphical Abstract

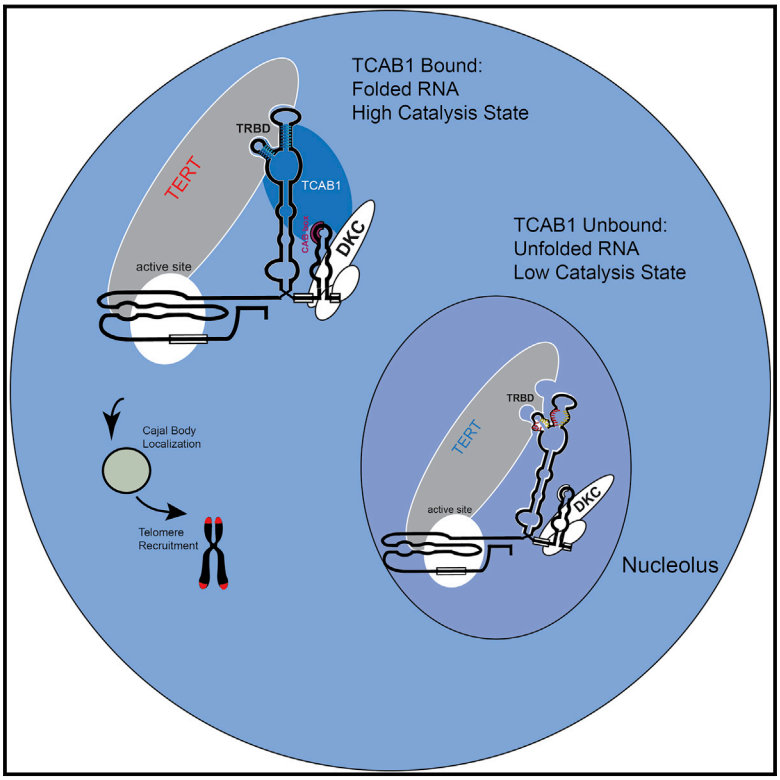

Highlights

- Telomerase catalytic activity is reduced in the absence of TCAB1
- TCAB1 directly stimulates catalytic activity of the assembled telomerase complex
- TCAB1 controls folding of CR4/5, a distal domain in the telomerase RNA component
- An RNA activity switch in telomerase toggled by TCAB1 controls telomerase activity

Authors

Lu Chen, Caitlin M. Roake, Adam Freund, ..., Rhiju Das, Howard Y. Chang, Steven E. Artandi

Correspondence

sartandi@stanford.edu

In Brief

The holoenzyme protein TCAB1 stimulates telomerase activity by shaping the conformation of a telomerase RNA activity switch.

Chen et al., 2018, Cell *174*, 1–13
June 28, 2018
https://doi.org/10.1016/j.cell.2018.04.039

CellPress

Please cite this article in press as: Chen et al., An Activity Switch in Human Telomerase Based on RNA Conformation and Shaped by TCAB1, Cell (2018), https://doi.org/10.1016/j.cell.2018.04.039

Article

Cell

An Activity Switch in Human Telomerase Based on RNA Conformation and Shaped by TCAB1

Lu Chen,[1,2,3] Caitlin M. Roake,[1,2,3] Adam Freund,[1,2,3] Pedro J. Batista,[4] Siqi Tian,[2] Yi A. Yin,[1,2,3] Chandresh R. Gajera,[1,2,3] Shengda Lin,[1,2,3] Byron Lee,[4] Matthew F. Pech,[1,2,3] Andrew S. Venteicher,[1,2,3] Rhiju Das,[2] Howard Y. Chang,[4] and Steven E. Artandi[1,2,3,5,*]

[1]Department of Medicine, Stanford University School of Medicine, Stanford, CA 94305, USA
[2]Department of Biochemistry, Stanford University School of Medicine, Stanford, CA 94305, USA
[3]Stanford Cancer Institute, Stanford University School of Medicine, Stanford, CA 94305, USA
[4]Center for Personal Dynamic Regulomes and Program in Epithelial Biology, Stanford University School of Medicine, Stanford, CA 94305, USA
[5]Lead Contact
*Correspondence: sartandi@stanford.edu
https://doi.org/10.1016/j.cell.2018.04.039

SUMMARY

Ribonucleoprotein enzymes require dynamic conformations of their RNA constituents for regulated catalysis. Human telomerase employs a non-coding RNA (hTR) with a bipartite arrangement of domains—a template-containing core and a distal three-way junction (CR4/5) that stimulates catalysis through unknown means. Here, we show that telomerase activity unexpectedly depends upon the holoenzyme protein TCAB1, which in turn controls conformation of CR4/5. Cells lacking TCAB1 exhibit a marked reduction in telomerase catalysis without affecting enzyme assembly. Instead, TCAB1 inactivation causes unfolding of CR4/5 helices that are required for catalysis and for association with the telomerase reverse-transcriptase (TERT). CR4/5 mutations derived from patients with telomere biology disorders provoke defects in catalysis and TERT binding similar to TCAB1 inactivation. These findings reveal a conformational "activity switch" in human telomerase RNA controlling catalysis and TERT engagement. The identification of two discrete catalytic states for telomerase suggests an intramolecular means for controlling telomerase in cancers and progenitor cells.

INTRODUCTION

Renewing tissues and cancers depend upon telomerase, a multisubunit ribonucleoprotein (RNP) enzyme, for long-term proliferation by maintaining telomeres, the nucleoprotein structures that protect chromosome ends (Pfeiffer and Lingner, 2013). Inactivating germline mutations in telomerase genes cause the human syndrome dyskeratosis congenita, characterized by tissue failure, including pulmonary fibrosis, aplastic anemia, and liver cirrhosis (Armanios and Blackburn, 2012). In contrast, telomerase upregulation is central to carcinogenesis, a step often controlled by highly recurrent somatic promoter mutations that upregulate TERT (Horn et al., 2013; Huang et al., 2013; Killela et al., 2013). Despite the critical importance of telomerase regulation in carcinogenesis and in tissue stem cells, mechanisms governing telomerase regulation in living cells remain incompletely understood.

Telomerase requires discrete steps that control enzyme assembly, trafficking in the nucleus and catalysis. These steps are organized around the telomerase RNA component (TR) that serves as a scaffold for the enzyme complex and encodes the template for reverse transcription during catalytic extension of telomeres (Schmidt and Cech, 2015). Most eukaryotic TRs share a conserved pseudoknot/template (PK/T) domain and a three-way junction element (CR4/5 domain), each forming independent but essential interactions with TERT (Mitchell and Collins, 2000; Podlevsky and Chen, 2016). The pseudoknot is essential for catalysis and folds into a triple helical structure proposed to position the template in the active site of the enzyme or to facilitate RNP assembly (Cash and Feigon, 2017). Within the CR4/5 domain, which binds the telomerase RNA binding domain (TRBD) of TERT, the P6.1 helix represents the most conserved sequence and serves a critical role in catalysis and in TERT association (Chen et al., 2002; Huang et al., 2014; Mitchell and Collins, 2000). Engineered mutations in P6.1 that disrupt base-pairing of the helix cause a marked reduction in both TERT binding and in telomerase catalytic activity (Chen et al., 2002; Robart and Collins, 2010). Mutations that restore base pairing rescue enzyme activity, whereas changes in helical length disrupt activity indicating that a P6.1 helix of optimal length is essential for telomerase function.

Studies of human telomerase *in vitro* using hTR fragments mixed with recombinant TERT protein have revealed that the PK/T domain together with TERT is insufficient to yield enzymatic activity, unless a CR4/5 fragment is added in *trans* (Mitchell and Collins, 2000). This ability of CR4/5 to stimulate activity of a minimal PK/T RNA fragment led the proposal that the CR4/5 serves as an "activation domain," enhancing the catalytic function of the enzyme (Leeper and Varani, 2005). This bipartite organization within the telomerase RNA and the presence of a distal activation

domain similar to CR4/5 is widely conserved in evolution (Podlevsky and Chen, 2016). Despite this broad conservation, the mechanisms underlying the cooperative interactions between the PK/T domain and the CR4/5 domain remain unknown. Structural studies show that engagement of the CR4/5 domain by the TERT TRBD in medaka fish induces a marked rearrangement of the P6.1 stem loop by more than 180 degrees to accommodate the TRBD protein surface. In the co-crystal structure, P6.1 and the adjacent P6 RNA helix of the CR4/5 domain form a clamp that binds a protrusion from the TRBD domain of TERT (Huang et al., 2014). Thus, the ability of the CR4/5 domain to operate in *trans*, together with the marked rearrangement of the P6.1 domain upon engaging the RNA binding domain of TERT suggests that CR4/5 facilitates enzymatic activity of telomerase through a conformational change in the complex (Huang et al., 2014; Kim et al., 2014; Robart and Collins, 2010).

Vertebrate TRs evolved a third element, the scaRNA domain, coopted from small Cajal body (sca) RNAs and related small nucleolar (sno) RNAs, noncoding RNAs involved in posttranscriptional modification of splicing and ribosomal RNAs, respectively. Within the scaRNA domain, the H/ACA element is bound by the dyskerin core complex, which coordinates assembly and stability of human TR (hTR) (Mitchell et al., 1999). A Cajal body box (CAB box), comprising the terminal hairpin loop of the scaRNA domain, mediates trafficking of telomerase and scaRNAs to Cajal bodies, nuclear sites of RNP modification and assembly (Cristofari et al., 2007; Jády et al., 2004; Zhu et al., 2004). CAB boxes in telomerase and in scaRNAs are bound by TCAB1, a WD40 repeat protein that controls localization of telomerase and scaRNAs within Cajal bodies (Tycowski et al., 2009; Venteicher et al., 2009). Depletion of TCAB1 using RNA interference impairs trafficking to Cajal bodies, mislocalizes telomerase to nucleoli, and causes telomeres to shorten (Freund et al., 2014; Venteicher et al., 2009; Zhong et al., 2011). Biallelic germline mutations in TCAB1 occur in a subset of patients with dyskeratosis congenita and cause mislocalization of telomerase from Cajal bodies to nucleoli in patient lymphoblasts and in patient-derived induced pluripotent stem cells (iPSCs) (Batista et al., 2011; Zhong et al., 2011). Although telomerase localizes to Cajal bodies and disruption of this localization by TCAB1 inhibition impairs telomerase function, it remains unclear whether Cajal body localization is the principal mechanism by which TCAB1 supports telomerase function.

TCAB1 depletion using RNA interference also disrupts telomerase recruitment to telomeres, a downstream step in telomerase action (Freund et al., 2014; Stern et al., 2012; Zhong et al., 2012). Recruitment of telomerase enzyme to telomeres is primarily controlled by a physical interaction between the TEN domain of TERT and the OB-fold domain of the telomere-binding protein TPP1 (Abreu et al., 2010; Nandakumar et al., 2012; Sexton et al., 2014; Zhong et al., 2012). Substitution of the telomerase scaRNA domain by heterologous RNA elements enabled stable expression of the chimeric hTR molecule, but this chimeric hTR did not support catalytic activity without overexpressing TERT protein (Vogan et al., 2016). This finding supported the importance of the dyskerin core complex and/or TCAB1 in facilitating telomerase assembly or catalytic function. Thus, TCAB1 binding to the scaRNA domain of hTR serves at least two essential functions in telomerase: one role in facilitating proper localization of telomerase within Cajal bodies and a second role in enhancing recruitment to telomeres.

To understand the molecular function of TCAB1 and the CAB box of the scaRNA domain in telomerase function, we inactivated TCAB1 in human cancer cells, human embryonic stem cells (ESCs) and mouse embryo fibroblasts (MEFs). We find that TCAB1 is unexpectedly required for catalytic activity of telomerase by facilitating proper folding of the hTR CR4/5 domain and optimal engagement with the TERT TRBD.

RESULTS

TCAB1 Loss Compromises Telomerase Activity in Human Cells and in Mouse Cells

To understand the importance of TCAB1 and Cajal body trafficking in telomerase function, we used genome editing with CRISPR/Cas9 to inactivate either TCAB1 or coilin, a Cajal body scaffold protein, in HeLa cells. Candidate knockout (KO) cell clones were screened by western blot and genomic DNA sequencing, resulting in six independent TCAB1-KO and six coilin-KO cell lines (Figure S1, upper and lower tables). Previous studies achieving only partial depletion of TCAB1 using short hairpin RNA (shRNA) revealed defects in telomere maintenance and in telomerase trafficking, but no effect on enzyme activity (Venteicher et al., 2009). In contrast, we found that a complete loss of TCAB1 protein resulted in a marked reduction in telomerase activity of approximately 80% in all HeLa TCAB1-KO clones, as measured by TRAP (telomere repeat amplification protocol) ($p < 1 \times 10^{-7}$, Student's t test) (Figure 1A, TRAP; Figure 1B quantification). TCAB1 protein was undetectable by western blot in each TCAB1-KO clone (Figure 1C). Lentiviral-based re-expression of tagged TCAB1 (3HA-TCAB1) in TCAB1-KO cells restored telomerase activity confirming a specific, reversible role for TCAB1 in enzyme function (A8 rescue, Figures 1A–1C). Coilin inactivation causes loss of Cajal bodies but often results in a relative preservation of pathways that depend upon Cajal-body concentrated processes (Tucker et al., 2001). In contrast to the diminished activity seen in TCAB1-KO cells, coilin inactivation caused a modest increase in telomerase activity (Figures 1A–1C). Thus, inactivation of TCAB1 but not coilin impairs telomerase activity in human cancer cells.

To study the effects of TCAB1 mutation in primary cells, we engineered *Tcab1* conditional knockout mice in which exons 4–6, encoding the first three WD40 repeats, were flanked by loxP sites. *Tcab1*$^{flox/null}$ or *Tcab1*$^{+/+}$ MEFs were treated with adenovirus expressing either GFP or a Cre-GFP fusion protein (Figures S2 and 1D–1F). TCAB1 protein was specifically lost in TCAB1$^{flox/null}$ MEFs treated with adeno-Cre-GFP by immunoblot using anti-mouse TCAB1 antibodies (Figure 1F). TCAB1 deletion led to a 77% reduction ($p < 0.005$, Student's t test) in TRAP activity in two independently derived *Tcab1*$^{loxP/null}$ MEF cultures when treated with adeno-Cre-GFP, compared with adeno-GFP (Figures 1D and 1E). In iPSCs derived from a dyskeratosis congenita patient with biallelic point mutations in TCAB1, hTR mislocalizes to nucleoli and telomere elongation with reprogramming is abrogated (Batista et al., 2011). To understand the effects of complete loss of TCAB1 in H1 human ESCs, we

Please cite this article in press as: Chen et al., An Activity Switch in Human Telomerase Based on RNA Conformation and Shaped by TCAB1, Cell (2018), https://doi.org/10.1016/j.cell.2018.04.039

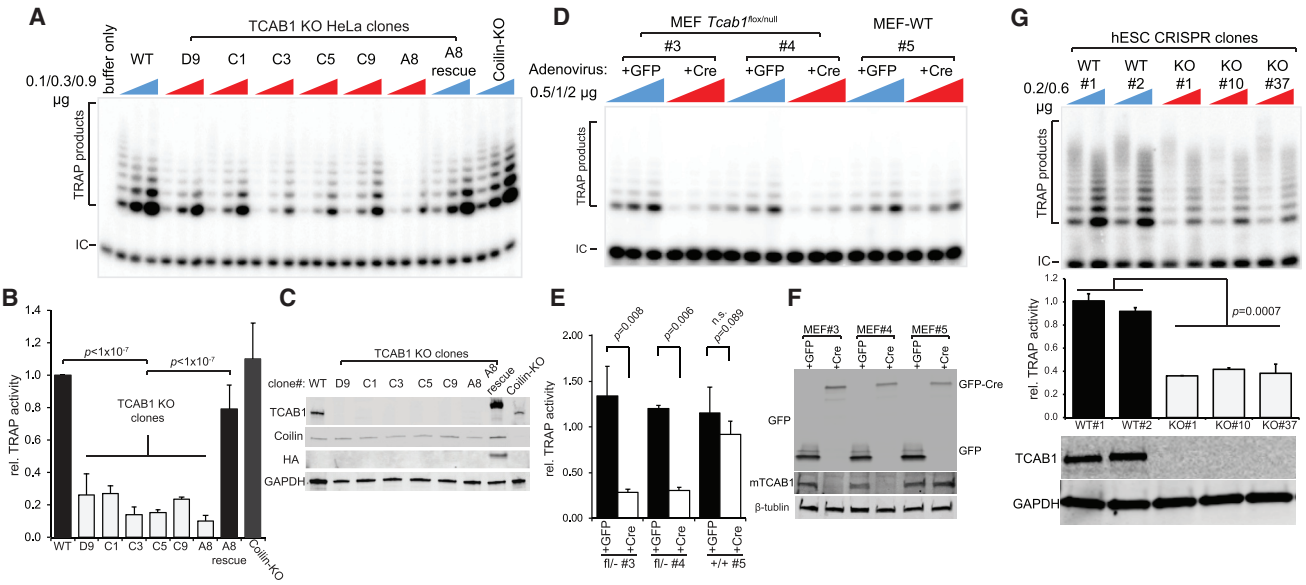

Figure 1. TCAB1 Loss Compromises Telomerase Activity in Human Cells and in Mouse Cells

(A) Telomerase activity by TRAP in TCAB1-KO HeLa cell clones generated by CRISPR/Cas9-mediated genome editing. A8 rescue, TCAB1-KO clone A8 stably expressing 3HA-TCAB1. WT, parental HeLa culture. Coilin-KO, HeLa clone with coilin disrupted. IC, internal control for PCR efficiency. Gel representing five repeats is shown.

(B) Quantification of telomerase activity in (A), values normalized to WT. Mean ± SEM was derived from three experiments, $p < 1 \times 10^{-7}$ for the average activity of all six TCAB1-KO clones versus WT control and A8 rescue by two-tailed Student's t test.

(C) Western blotting of HeLa whole-cell extracts assayed by TRAP in (A).

(D) Telomerase activity by TRAP in TCAB1$^{flox/null}$ (embryo#3, #4) or TCAB1$^{+/+}$ (embryo#5) MEFs treated with adenovirus expressing either GFP or GFP-Cre fusion. Gel representing three repeats is shown.

(E) Quantification of telomerase activity in (D). Mean ± SEM derived from three experiments. p value for GFP versus Cre in each line by two-tailed Student's t test.

(F) Western blotting of MEF whole-cell extracts assayed in (D). Primary antibodies: anti-GFP (top panel), anti-mouse TCAB1 (middle), anti-tubulin (bottom).

(G) Telomerase activity by TRAP in TCAB1-KO hESC clones generated by CRISPR/Cas9-mediated genome editing (upper). Quantification of telomerase activity (middle) based on three repeats. p value of KO versus WT clones is 0.0007 by two-tailed Student's t test. Western blot for TCAB1 protein (lower).

See also Figures S1, S2, and S4.

generated TCAB1 ESC KO clones. Candidate clones were identified by genomic sequencing (Figure S1, middle table) and shown to lack TCAB1 protein by immunoblot (Figure 1G). Telomerase activity was reduced by 64% in three independent TCAB1-KO human embryonic stem cells (hESCs) clones compared to parental H1 ES clones (p = 0.0007) (Figure 1G). These data show that genetic knockout of TCAB1 impairs telomerase enzymatic activity in human cancer cells, primary mouse cells, and human ESCs, indicating a conserved role for TCAB1 in supporting telomerase enzymatic function.

TCAB1 Loss Impairs Trafficking, Recruitment to Telomeres, and Telomere Maintenance Independent of Fully Assembled Cajal Bodies

Telomerase localizes within Cajal bodies in fixed cells (Jády et al., 2004; Zhu et al., 2004), and live-cell imaging showed that TERT exhibits extended residence time in Cajal bodies (Schmidt et al., 2016). To understand the localization of telomerase in TCAB1-KO cells, we performed RNA fluorescence in situ hybridization (FISH) for hTR together with immunostaining for coilin. Analysis of telomerase trafficking in TCAB1-KO HeLa cell clones revealed that hTR was no longer present in Cajal bodies and mislocalized to nucleoli (Figure S3A), as demonstrated previously through depletion of TCAB1 (Venteicher et al., 2009; Zhong et al., 2011). Coilin-positive Cajal bodies were preserved in TCAB1-KO cells, indicating that TCAB1 is not required for Cajal body formation. In contrast, Cajal bodies were not readily detected and hTR was diffusely nuclear in coilin-KO cells (Figure S3A).

To understand differential roles of TCAB1 and coilin in telomerase recruitment, we overexpressed both Flag-TERT and hTR by transient transfection in HeLa cells and HeLa cells lacking TCAB1 or coilin. Telomerase was effectively recruited to telomeres in parental HeLa cells based on either combined hTR RNA FISH and TRF2 immunostaining (Figure 2A), or co-staining for Flag-TERT and telomeres by DNA FISH (Figure S3B). At the same time, neo-Cajal bodies containing coilin and TCAB1 appear at telomeres (Figures 2B and 2C) (Zhong et al., 2012). Loss of TCAB1 caused a quantitative reduction in recruitment of telomerase to telomeres, based on staining for hTR by RNA FISH or Flag-TERT by immunostaining (Figures 2A, 2D, S3B, and S3C), and concomitant progressive shortening of telomeres (Figure 2E). Loss of coilin caused a marked suppression of telomerase foci at telomeres (Figures 2A, 2D, S3B, and S3C), but telomeres were effectively maintained (Figure 2E) (Chen et al., 2015; Vogan et al., 2016). Inhibition of telomerase foci in

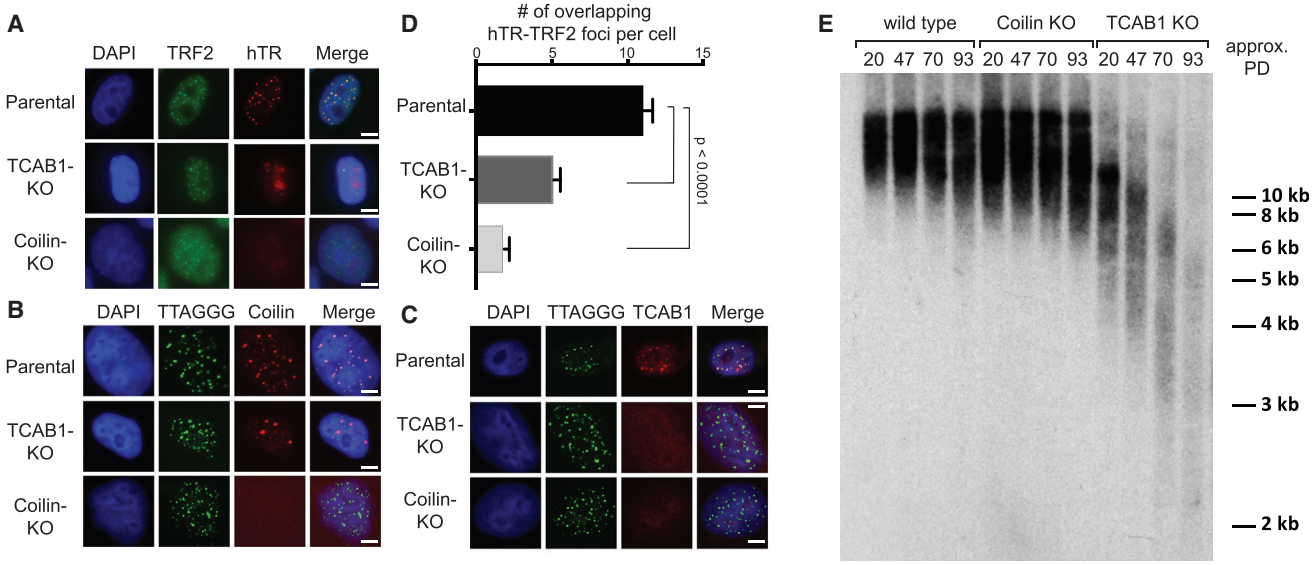

Figure 2. TCAB1 Loss Impairs Recruitment to Telomeres and Telomere Maintenance Independent of Fully Assembled Cajal Bodies

(A–C) Telomerase recruitment to telomeres assayed by overexpressing Flag-TERT and hTR in parental HeLa cells, TCAB1-KO HeLa cells and coilin-KO HeLa cells. (A) Combined IF for TRF2 and RNA FISH for hTR; (B) combined IF for coilin and DNA FISH for telomere repeats; (C) combined IF for TCAB1 and DNA FISH for telomere repeats. Scale bars, 5 μm source data.

(D) Quantification of mean number of hTR foci co-localized with telomeres marked by TRF2. For each genotype, >70 nuclei were scored for the number of hTR foci at telomeres. Error bars, SEM. Student's t test, $p < 0.0001$.

(E) Telomere lengths measured by TRF Southern blot in parental HeLa cells and TCAB1-KO and Coilin-KO clones with cell passage. PD, population doublings. See also Figure S3.

coilin-KO cells therefore indicates an absence of neo-Cajal bodies, rather than diminished recruitment. The differential effects of TCAB1 loss and coilin loss on telomere maintenance and telomerase recruitment suggest that the required role for TCAB1 in telomerase function does not necessitate a fully assembled Cajal body (Figure 2E). Taken together, these data show that TCAB1 loss impairs telomerase recruitment to telomeres, disrupts telomerase localization to Cajal bodies, and provokes progressive telomere shortening.

Preserved RNP Processivity and Assembly of the TERT-hTR Catalytic Core in Cells Lacking TCAB1

To determine whether a defect in assembly of the catalytic core of telomerase underlies the impairment in enzyme catalysis in TCAB1-KO cells, we affinity purified endogenous telomerase RNP complexes from nuclear extracts using a rabbit polyclonal anti-TERT antibody that we developed previously (Venteicher et al., 2008). Pull-down of endogenous telomerase in this manner depleted approximately 75% of the active enzyme (Figure S4A). To measure the catalytic activity of the purified enzymes, we employed the direct primer extension assay for telomerase activity in which the purified telomerase acts on a telomere substrate oligonucleotide in the presence of radioactive nucleotides. Catalytic activity of purified telomerase complexes from three independent TCAB1-KO clones were reduced by 80% compared to purified enzyme from parental HeLa cells (Figure 3A quantified in Figure 3B). This catalytic defect was rescued in telomerase affinity-purified from TCAB1-KO cells with restored TCAB1 protein. Consistent with the TRAP assays, catalytic activity of telomerase affinity-purified from coilin-KO cells was modestly increased as measured by the direct primer extension assay (Figures 3A and 3B). To examine whether the catalytic defect in TCAB1-KO cells is due to reduced telomerase repeat addition processivity, we plotted normalized intensity of each telomere extended species over the repeat number (Figure 3A) and derived the processivity value $R_{1/2}$ (Figure 3C), which represents the number of repeats synthesized before half of the chains have dissociated (Chen et al., 2018; Wang et al., 2007). We found no significant processivity difference among all RNPs regardless of its TCAB1 status. In addition, we found no consistent change in hTR accumulation in TCAB1-KO HeLa cell clones by northern blot (Figure 3D), and no reduction in mTR (mouse TR, Figure S4B) or TERT mRNA in TCAB1-null MEFs (Figure S4C). In each of the affinity-purified complexes, we assayed the amount of TERT protein and hTR RNA by western blot and northern blot, respectively. Levels of immunoprecipitated TERT protein and hTR RNA were similar when telomerase was isolated from parental HeLa cells, TCAB1-KO cells, and coilin-KO cells, indicating that TCAB1 is not required for assembly of the catalytic core of telomerase (Figure 3D). Overall, these data show that TCAB1 loss causes a reduced rate of enzymatic activity without compromising RNP processivity or assembly of the catalytic core.

TCAB1 Stimulates Telomerase Activity through an Interaction with the CAB Box

To test whether TCAB1 directly stimulates catalysis of the assembled enzyme, we performed *in vitro* add-back of recombinant TCAB1 to purified telomerase RNPs lacking TCAB1

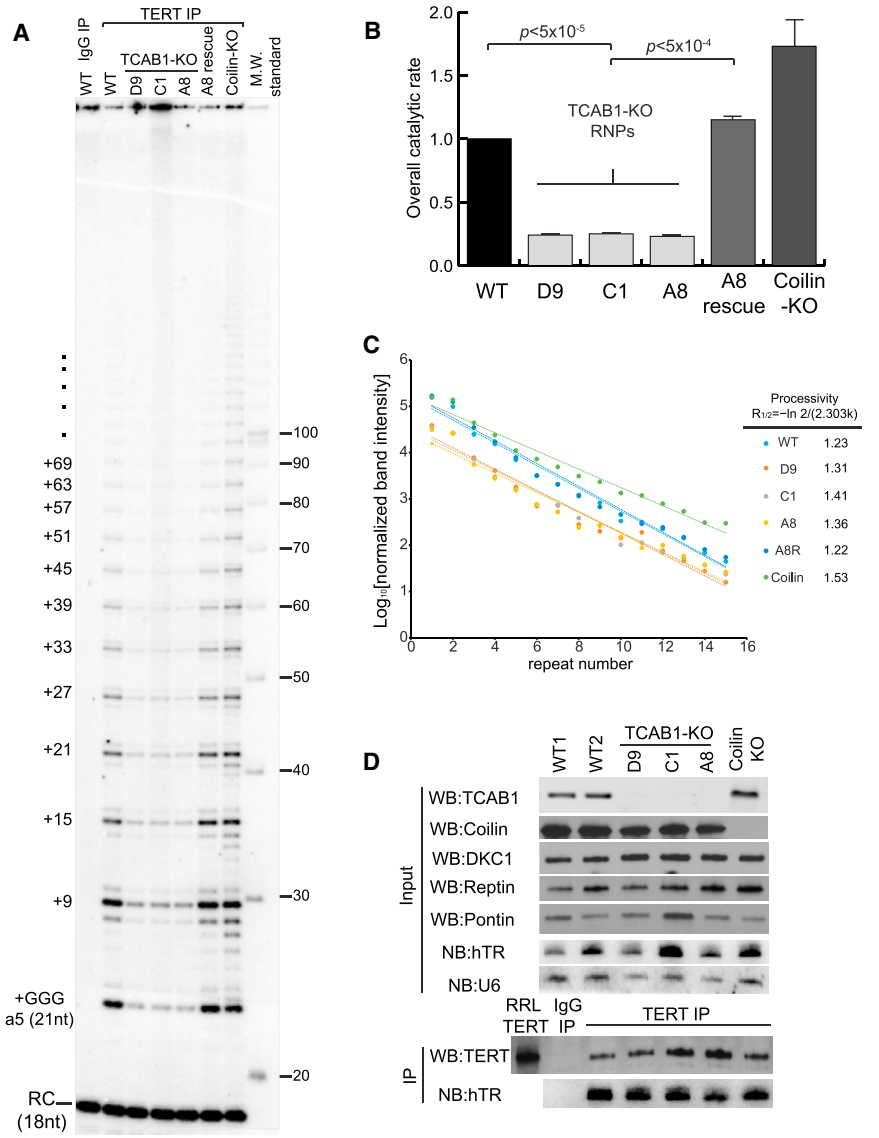

Figure 3. Impaired Catalysis but Preserved Assembly of the TERT-hTR Catalytic Core in Cells Lacking TCAB1

(A) Direct telomerase primer extension assay on endogenous telomerase RNPs immunopurified from indicated nuclear extracts using polyclonal anti-TERT antibodies. WT, parental HeLa cells; TCAB1-KO, clones D9, C1, A8; A8 rescue, TCAB1-KO clone A8 stably expressing 3HA-TCAB1; Coilin-KO. WT immunoglobulin G (IgG) IP, non-specific IgG for IP with parental HeLa extract. MW standard,100-nt DNA ladder. a5 (21nt)+GGG, telomeric DNA primer a5 plus three labeled guanines; additional extension products indicated by number of residues added. RC, recovery control. Gel image represents three independent experiments.

(B) Overall catalytic rate, relative rate of incorporation of ^{32}P-GMP per RNP, measured by combining the intensity of all extended bands within the indicated gel lane (A). Values were normalized to WT RNP. Mean ± SEM derived from 3 experiments; $p < 5 \times 10^{-5}$ TCAB1-KO versus parental HeLa, $p < 5 \times 10^{-4}$ TCAB1-KO versus A8 rescue by two-tailed Student's t test.

(C) Repeat addition processivity measured from Figure 3A. Intensity of each telomeric band was measured, normalized by the number of ^{32}P-GMP incorporated, and plotted versus the corresponding repeat number. Repeat addition processivity ($R_{1/2}$) measures the number of repeats synthesized before 50% enzymes have dissociated, which follows the equation:

$$R_{1/2} = \frac{-\ln 2}{2.303k}$$

where k = slope.

(D) Assembly of telomerase catalytic core assayed by IP of TERT and northern blot for hTR. Endogenous telomerase RNPs from (A) were assayed. Input, indicated proteins assayed by western blot; hTR and U6 RNAs assayed by northern blot. IP, telomerase RNPs immunopurified using TERT antibodies were assayed by western blot for TERT protein and by northern blot for hTR. RRL TERT, rabbit reticulate lysate (RRL)-expressing 3xFlag tagged TERT protein. IgG IP, non-specific IgG used for IP.

See also Figure S4

(Figure 4A). Because TCAB1 binds scaRNAs and other RNAs in addition to telomerase (Tycowski et al., 2009; Venteicher et al., 2009), we isolated 3HA-TCAB1 by affinity purification from HeLa nuclear extracts that were either left untreated or treated with RNase to degrade TCAB1-associated RNAs; subsequently, each sample was either eluted with peptide or left bead-bound, yielding four different 3HA-TCAB1 samples (Figures 4A and 4B). Each recombinant 3HA-TCAB1 fraction lacked telomerase activity on its own (Figure 4D, lanes 1–8). Both peptide-eluted and bead-bound preparations of 3HA-TCAB1 stimulated telomerase catalytic activity in a concentration-dependent manner. Stimulation of telomerase activity by 3HA-TCAB1 occurred only when the 3HA-TCAB1 extract had been pre-treated with RNase to degrade RNAs copurifying with 3HA-TCAB1 (Figure 4D, compare lanes 14, 16 and lanes 13, 15). These findings suggest that an RNA binding site on TCAB1 needs to be vacant to bind hTR and stimulate telomerase activity. TCAB1 binds hTR and other scaRNAs at a CAB box element, a conserved four nucleotide RNA motif in the scaRNA domain of these guide RNAs (Cristofari et al., 2007; Tycowski et al., 2009). To further test the requirement for RNA binding in TCAB1-mediated stimulation of telomerase activity, we employed a competition assay in which purified 3HA-TCAB1 was pre-incubated with an excess of hTR molecules synthesized *in vitro* (Figure 4C). Active RNase-treated 3HA-TCAB1 was pre-treated either with wild-type hTR or with hTR variants that each harbor a single nucleotide mutation known to disrupt binding of TCAB1 to the CAB-box element (CAB boxmu1 - G414C, CAB box mu2 – G412C) (Cristofari et al., 2007; Freund et al., 2014; Jády et al., 2004). Pre-incubation with wild-type hTR disrupted the ability of 3HA-TCAB1 to stimulate telomerase activity (Figure 4D, lanes 22–24), whereas pre-incubation with either CAB box mutant-form of hTR failed to block

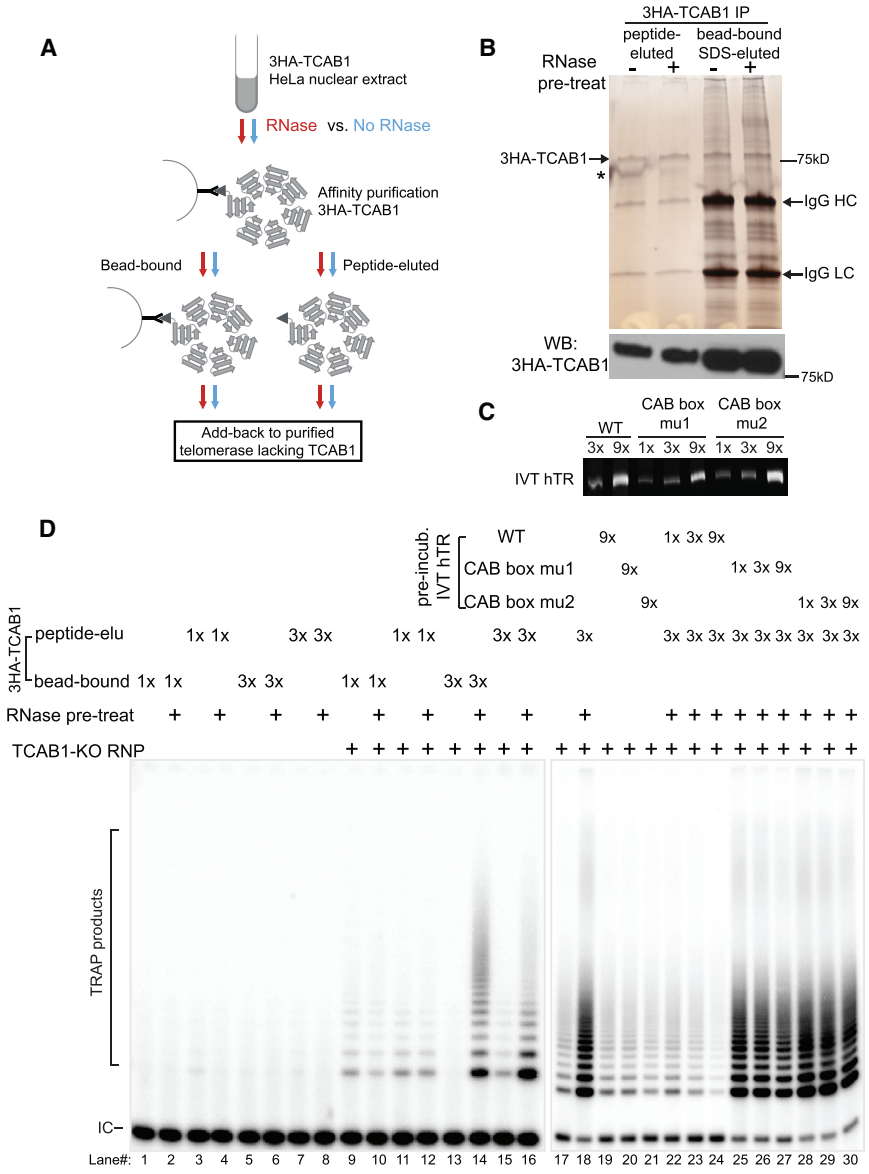

Figure 4. TCAB1 Stimulates Telomerase Activity through an Interaction with the CAB Box

(A) Schematics for biochemical reconstitution of various 3HA-TCAB1 fractions with telomerase RNP lacking TCAB1.

(B) Silver staining of purified recombinant 3HA-TCAB1 fractions by anti-HA affinity chromatography from A8 HeLa clone stably overexpressing 3HA-TCAB1. Extracts were either treated with RNase or left untreated and then affinity purified on anti-HA beads. Bead-bound 3HA-TCAB1 was either competitively eluted by 3xHA peptide or directly boiled in SDS sample buffer. Asterisk, BSA signal from adjacent lane.

(C) Ethidium bromide staining of *in vitro* transcribed (IVT) RNAs: WT (wild-type) hTR, CAB box mu1 (G414C), and CAB box mu2 (G412C). 1×, 3×, 9× represent relative volumes loaded.

(D) Telomerase activity by TRAP when adding back recombinant 3HA-TCAB1 to affinity-purified telomerase lacking TCAB1, TCAB1-KO RNP. Telomerase complexes were affinity-purified using anti-TERT antibodies from A8 TCAB1-KO HeLa clones. Left: effect of add-back of indicated 3HA-TCAB1 fractions on telomerase activity of purified TCAB1-KO telomerase RNP. Right: effect of pre-incubating recombinant 3HA-TCAB1 with *in vitro* transcribed hTRs (from C) prior to the addition of telomerase RNPs and telomerase substrates. Gel representative of three independent repeats.

the activity of 3HA-TCAB1 in enhancing enzyme catalysis (Figure 4D, lanes 25–30). These results show that an intact CAB box in hTR is required to block the stimulating effect of 3HA-TCAB1 on telomerase activity, supporting the model that TCAB1 stimulates telomerase activity through direct binding of the hTR CAB box. These data show that TCAB1 promotes telomerase catalytic function through direct binding of hTR after assembly of the enzyme catalytic core.

TCAB1 Drives Regional RNA Folding in an hTR Domain Critical for Catalysis

The diminished activity of telomerase in the absence of TCAB1, coupled with the *in vitro* stimulation of telomerase in add-back studies, suggests that TCAB1 directly executes a change in the telomerase complex. To understand whether the stimulatory effect of TCAB1 on telomerase activity is mediated through alterations in hTR secondary structure (Figure 5A), we employed a variant of selective 2′-hydroxyl acylation and profiling experiment-seq (icSHAPE) (Flynn et al., 2016). Endogenous telomerase complexes were isolated by TERT-immunoprecipitation (IP) from nuclear extracts derived from parental HeLa cells, TCAB1-KO cells, and TCAB1-KO cells rescued by stable expression of TCAB1 (TCAB1-KO genetic rescue). Immobilized complexes were treated with NAI-N_3 (2-methylnicotinic acid imidazolide azide) to acylate flexible RNA 2′-OH residues, followed by isolation of modified RNA sequences, biotinylation, reverse transcription, library construction, and deep sequencing (Figure S5A, schematic). Sequencing data were used to derive a flexibility score at each nucleotide of hTR from each RNP analyzed, and these reactivity scores were plotted on the linear sequence of hTR (Figure 5B). To compare hTR structures from cells with and without TCAB1, we subtracted the wild-type telomerase RNP icSHAPE reactivity scores from the TCAB1-KO RNP reactivity score and plotted these reactivity difference values on the secondary structure model of hTR obtained from the telomerase database (Figure 5C, left) (Podlevsky et al., 2008).

icSHAPE reactivity profiles of the catalytically indispensable PK/T domain were similar comparing the three distinct RNPs (Figure S5B). Reactivities within the remaining hTR structure

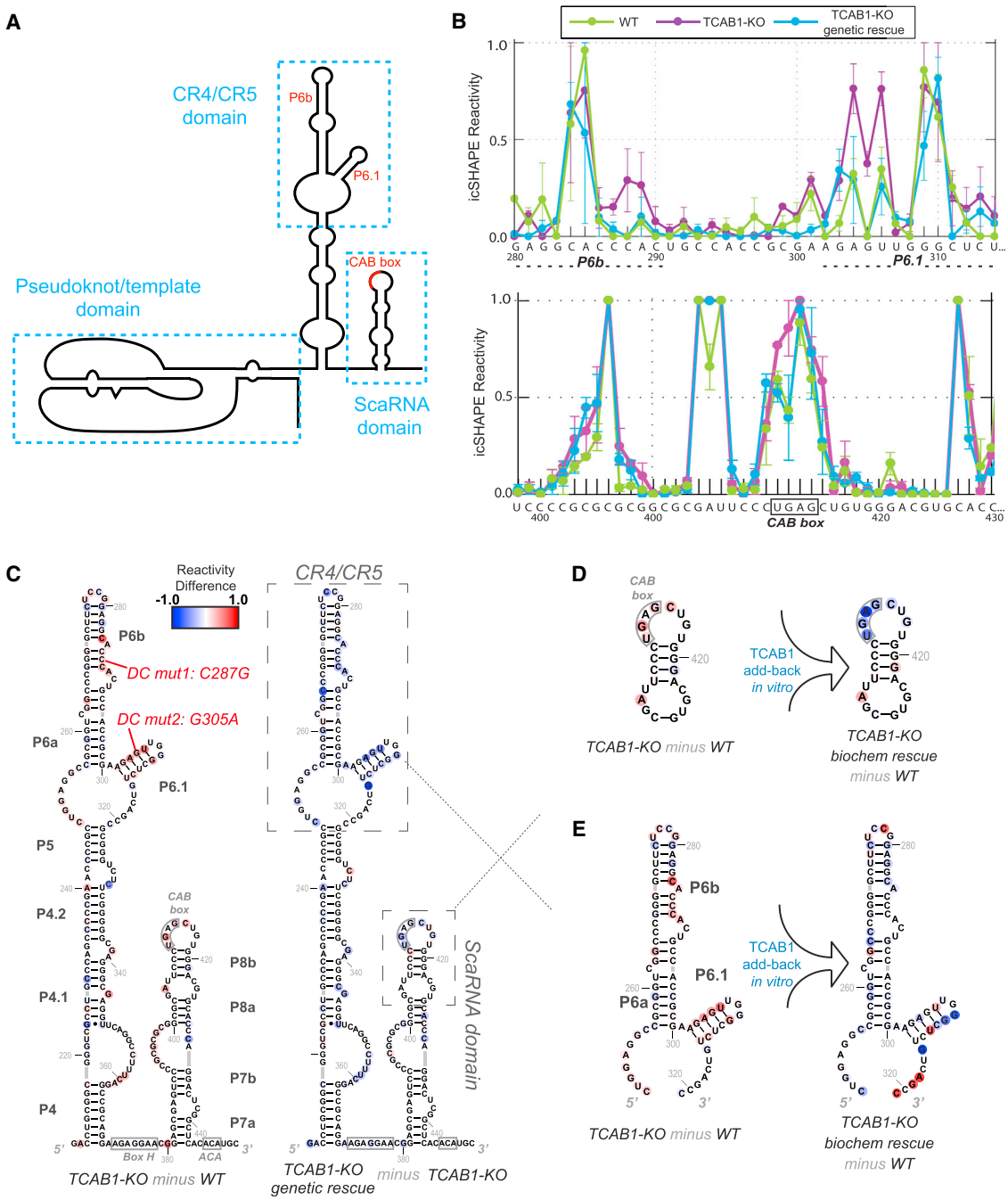

Figure 5. TCAB1 Drives Regional RNA Folding in an hTR Domain Critical for Catalysis

(A) Domain composition of the telomerase RNA hTR. Individual domains are framed in rectangles. hTR motifs affected by TCAB1 are labeled in red.

(B) Affinity-purified endogenous telomerase RNPs were subject to chemical modification and mapping of residue flexibility using icSHAPE. Relative icSHAPE reactivity comparing affinity-purified telomerase RNAs from parental HeLa cells (WT), TCAB1-KO (A8), and A8 rescue with stable overexpression of TCAB1 (TCAB1-KO genetic rescue). Regions of reactivity affected by TCAB1 are shown. Error bars represent the SD of icSHAPE values obtained from two technical replicates. x axis, primary hTR sequence.

(C) icSHAPE reactivity difference scores derived comparing two telomerase RNPs and mapped onto hTR secondary structure at each nucleotide position. Increased reactivity difference is plotted in red color; decreased reactivity difference in blue. The specific RNPs compared are indicated below each structure. DC mut1 and mut2 are hTR mutations isolated from dyskeratosis congenita patients in P6b and P6.1, respectively.

(D and E) icSHAPE reactivity difference scores at CAB box region (D) and CR4/5 domain (E) of hTR upon add-back of recombinant 3HA-TCAB1 to affinity purified telomerase lacking TCAB1. RNase pre-treated, eluted 3HA-TCAB1 (Figure 4B) was incubated with TCAB1-KO RNPs prior to the addition of icSHAPE modifier *in vitro*. See also Figures S5 and S6.

were largely comparable (Figure S6), with two exceptions—the CAB box and the CR4/5 domain critical for telomerase catalytic function distal from the CAB box in linear sequence and secondary structure (Figure 5B). Reactivity was increased in the CAB box of telomerase isolated from TCAB1-KO cells, consistent with this loop representing the TCAB1 binding site on hTR (Figure 5C, left; red, increased flexibility; blue, decreased flexibility).

TCAB1 loss was associated with increased icSHAPE reactivity in two helices within CR4/5, P6.1, and P6b, consistent with local unfolding of P6.1 and P6b in telomerase from TCAB1-KO cells compared with telomerase from parental cells (Figures 5B and 5C, left). Restoration of TCAB1 protein in TCAB1-KO genetic rescue cells reversed these structural changes in the CAB box and in P6.1 and P6b (Figure 5C, right). Note that genetically restoring TCAB1 to TCAB1-KO cells resulted in complementary structural changes in hTR compared with eliminating TCAB1 protein (Figure 5C, left versus right). To determine whether this role for TCAB1 in folding P6.1 and P6b is direct, we incubated recombinant 3HA-TCAB1 protein with purified telomerase RNP complexes from TCAB1-KO cells prior to the addition of icSHAPE chemical modification. *In vitro* add-back of 3HA-TCAB1 suppressed icSHAPE reactivity at the CAB box, reversing the increased reactivity seen in the telomerase complex from TCAB1-KO cells (Figure 5D). Furthermore, addition of recombinant 3HA-TCAB1 protein *in vitro* to the purified TCAB1-KO telomerase RNP suppressed the structural changes in P6.1 and P6b in the CR4/5 domain caused by TCAB1 loss (Figure 5E). Together, these structure profiling results demonstrate that loss of TCAB1 leads to unexpected unfolding in the hTR CR4/5 domain, distant from the TCAB1 binding site in secondary structure, and that recombinant TCAB1 promotes refolding of this RNA domain *in vitro*.

Impaired hTR CR4/5-TERT Association in TCAB1 Knockout Cells and in Patient-Derived hTR Mutants

Within CR4/5 domain of hTR, the TCAB1-dependent P6.1 and P6b helices serve poorly understood functions in enhancing telomerase activity (Mitchell and Collins, 2000; Podlevsky and Chen, 2016). The P6.1 stem loop is essential for telomerase activity, and mutations that disrupt base pairing in the stem impair both activity and binding to the TRBD of TERT (Chen et al., 2002; Robart and Collins, 2010). The P6b helix is also important for catalytic activity, as deletions in CR4/5 compromising P6b abrogate telomerase activity (Mitchell and Collins, 2000). We noted that in dyskeratosis congenita patients, two germline mutations in CR4/5 had been described—G305A (Robart and Collins, 2010; Yamaguchi et al., 2003) and C287G (Vulliamy et al., 2011)—and that these nucleotides reside within the P6.1 and P6b helices folded by TCAB1 (red lines, Figure 5C). We hypothesized that each of the mutations in P6.1 and P6b may compromise the function of these domains in a similar manner to that of TCAB1 loss. To address this question, we expressed 3Flag-TERT together with wild-type hTR, G305A hTR or C287G hTR in 293T cells and analyzed catalytic activity of the purified RNPs (Figure S7A). Using the direct primer extension assay, we found that telomerase activity from RNPs containing either G305A or C287G hTR alleles was markedly reduced (18% ± 4% and 2% ± 0.4%, respectively, compared with wild-type, $p < 0.0003$) (Figures 6A and 6B), consistent with previous findings (Mitchell and Collins, 2000; Robart and Collins, 2010; Vulliamy et al., 2011). To further interrogate the connection between TCAB1 and catalysis, we measured the activity of telomerase RNPs incorporating hTR molecules with mutations in the CAB box element where TCAB1 binds. Telomerase activity, but not processivity, was reduced in each CAB box mutant (57% ± 5% and 44% ± 2% in CAB box m1 versus CAB box m2) (Figures 6A–6C). The diminished activity seen in the CAB box mutant hTR variants is consistent with the reduced enzyme activity seen in TCAB1-KO cells. No processivity defect was observed in the mutant RNPs containing CR4/5 unfolding mutation G305A (Figure 6C). These data highlight the importance of P6.1 and P6b in telomerase activity and show that impairing TCAB1 function in the telomerase complex, either through loss of TCAB1 protein or by CAB box mutation each diminishes overall catalytic activity without affecting processivity. These findings suggest that mutations in hTR CR4/5 and disruption of TCAB1 function may operate through a common mechanism in impairing catalysis.

Based on the critical requirement for CR4/5 in binding TERT, we investigated whether impaired TERT association represented such a common mechanism. TERT binds to hTR through two independent interactions with the PK/T and the CR4/5 domain (Chen et al., 2002; Mitchell and Collins, 2000). Consistent with the importance of two independent hTR binding sites, overall TERT-hTR association was not altered in TCAB1-KO cells (Figure 3D). To overcome potential redundancy with two binding sites and to specifically probe the TERT-hTR CR4/5 interaction, we expressed Flag-TERT and fragments of hTR lacking the PK domain and template region (hTR-ΔPK, comprising residues 209∼451) in either TCAB1-KO HeLa cells or in TCAB1-KO cells rescued by transient expression of HA-TCAB1. Association of wild-type hTR-ΔPK with Flag-TERT was reduced by 68% in cells lacking TCAB1, as measured by IP northern (Figure 6D, lanes 1 and 6; Figure 6E, $p = 0.022$). This result indicates that TCAB1 facilitates the interaction between CR4/5 and TERT. Binding of C287G hTR-ΔPK to Flag-TERT was nearly undetectable in cells lacking or retaining TCAB1 expression, indicating that the P6b helix is required for binding TERT (Figure 6D, lanes 2 and 7; Figure 6E). Association of G305A hTR-ΔPK was reduced by 60% in cells that express TCAB1 ($p = 0.019$ compared with wild-type hTR-ΔPK). Loss of TCAB1 further diminished binding of G305A hTR-ΔPK with Flag-TERT (reduced by 86% of wild-type hTR-ΔPK binding in TCAB1-proficient cells, $p = 0.001$) (Figure 6D, lanes 3 and 8; Figure 6E). This result indicates that G305A mutation in hTR impairs TERT binding, and that TCAB1 loss further disrupts TERT association.

Binding of the CABm1-ΔPK and CABm2-ΔPK fragments to Flag-TERT in cells expressing TCAB1 was reduced by 32% and 76% ($p = 0.018$ and 0.002, respectively), indicating that CAB box mutations influence TERT association (Figure 6D, lanes 1, 4, and 9; Figure 6E). In contrast to wild-type hTR or G305A hTR, Flag-TERT association with CABm1-ΔPK and CABm2-ΔPK was not further reduced in TCAB1-KO cells (Figure 6D, lanes 4 and 5 and 9 and 10; Figure 6E; $p = 0.277$ and 0.357, respectively). These results indicate that the CAB box is required for efficient association between TERT and CR4/5 but that in the context of CAB box mutations TCAB1 loss causes no further

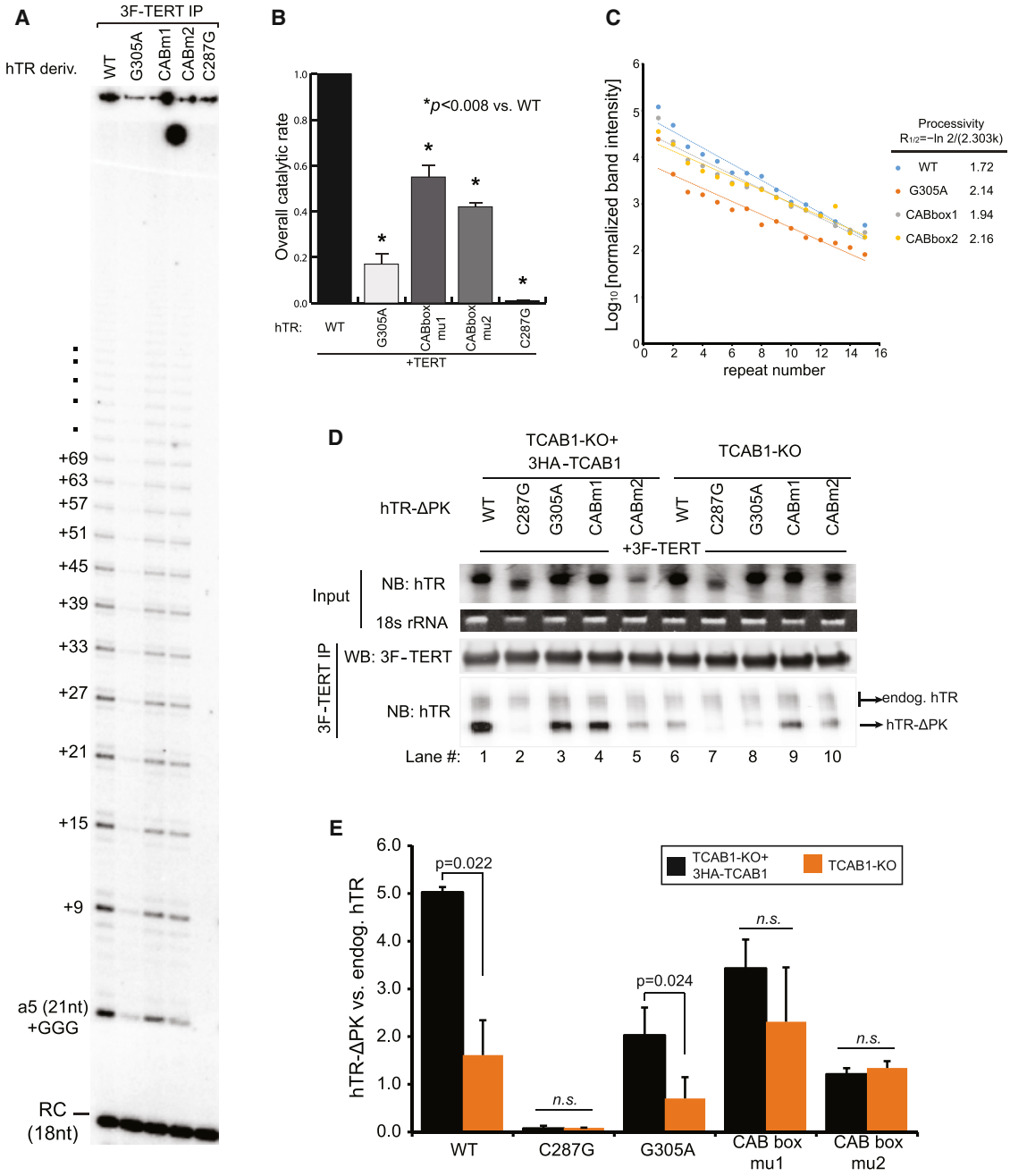

Figure 6. Impaired hTR CR4/5-TERT Association in TCAB1 Knockout Cells and in Patient-Derived hTR Mutants

(A) Direct telomerase primer extension assay on purified telomerase RNPs reconstituted in 293T cells by overexpressing 3x Flag epitope tagged TERT and indicated hTR derivatives. Telomerase complexes immunopurified on Flag antibody resin. Gel representative of three experiments is shown.

(B) Overall catalytic rate, relative rate of incorporation of ^{32}P-GMP per RNP, measured by combining the intensity of all extended bands within the indicated gel lane. Values were normalized to WT RNP. Mean ± SEM derived from 3 experiments; $p < 0.008$ for all hTR derivatives versus WT by two-tailed Student's t test.

(C) Repeat addition processivity calculation of (A), as detailed in Figure 3C.

(D) Association between 3Flag-TERT and hTR fragments in TCAB1-KO cells plus or minus TCAB1 expression. TCAB1-KO cells (A8) transiently transfected with plasmids expressing 3Flag-TERT and indicated hTR-ΔPK fragments (209–451) plus or minus 3HA-TCAB1 plasmid. Northern blotting of the Flag antibody-immunopurified fractions revealed a lower mobility band representing endogenous full-length hTR and higher mobility hTR-ΔPK fragments. Blots represent three independent experiments.

(E) Quantitation of the ratio between hTR-ΔPK fragments and endogenous full-length hTR (D). Mean ± SEM were derived from three experiments by two-tailed Student's t test.

See also Figure S7.

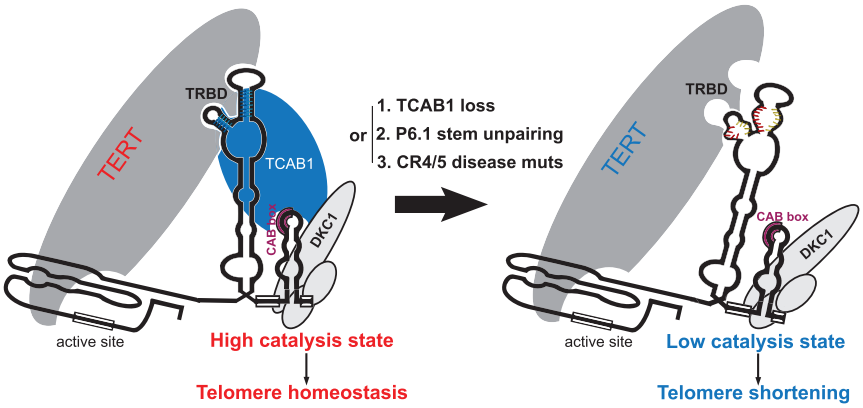

Figure 7. A Conformational Activity Switch in Telomerase RNA Shaped by TCAB1

An activity switch in human telomerase RNA based on RNA conformation controls telomerase catalytic activity. Human telomerase RNA is composed of three domains: a pseudoknot template domain in the active site, the CR4/5 domain that activates the enzyme, and the scaRNA domain harboring the H/ACA element and the CAB box. TCAB1 binds to the CAB box of hTR via its WD40 repeat domain and concentrates telomerase in Cajal bodies. While tethered to the CAB box, TCAB1 facilitates proper folding of RNA helices P6.1 and P6b within the CR4/5 domain and optimal engagement with the TERT TRBD domain. With a properly folded activity switch, telomerase is in a high catalytic state and telomeres are maintained. In the absence of TCAB1 (1), the activity switch is improperly folded resulting in a low catalytic state, impaired trafficking, and diminished recruitment, resulting in telomere shortening. Engineered mutation in P6.1 (2) or mutations in P6.1 or P6b from dyskeratosis congenita patients (3) disrupt the activity switch, mimicking the effects of TCAB1 loss.

reduction in TERT binding. Importantly, association of each hTR ΔPK fragment with HA-TCAB1 was dependent on the presence of an intact CAB box (Figure S7B). Taken together, these data show that TCAB1 loss causes unfolding in hTR CR4/5 and impairs binding between CR4/5 and TERT. The impaired association between CR4/5 and TERT in TCAB1-KO cells, together with the icSHAPE data provide independent, mutually reinforcing evidence that the conformation of CR4/5 is disrupted in the absence of TCAB1. The altered secondary structure in CR4/5 and impaired association with TERT likely explain the marked reduction in catalytic activity caused by loss of TCAB1. Our data reveal a critical role for TCAB1 in facilitating a conformational change in hTR in the CR4/5 domain that controls TERT association and catalytic function. We propose that these changes in CR4/5 conformation represent an "activity switch" that toggles telomerase between a low activity state and a high activity state. In the TCAB1-bound state, hTR association with TERT is enabled through proper conformation of the CR4/5 domain, resulting in elevated catalytic activity. In the TCAB1-free state, P6.1 and P6b helices become unfolded and TERT association is reduced, resulting in a low catalytic state.

DISCUSSION

An Activity Switch in the Telomerase RNA

Our current view of telomerase regulation is based primarily on changes in levels of TERT, hTR, or the assembled enzyme. Intrinsic changes within the assembled enzyme have not been explored. Our findings provide evidence for the existence of an activity switch within telomerase based on RNA conformation and controlled by TCAB1. In the absence of TCAB1, the telomerase enzyme core assembles but remains in a low catalytic state characterized by unfolding of the critical CR4/5 domain and diminished association between the CR4/5 domain and TERT (Figure 7). The preservation of catalytic core assembly in TCAB1-KO cells suggests that if TCAB1 associates with hTR prior to hTR-TERT assembly, TCAB1 is not required for this step. The ability of recombinant TCAB1 to enhance folding of the CR4/5 domain in the purified RNP suggests that TCAB1 may act *in vivo* at a step after TERT-hTR assembly. Either engineered mutations or patient-derived mutations within the CR4/5 hTR domain cause a similar disruption of catalytic function and TERT association (Figure 7). These hTR mutations and TCAB1 mutations seen in DC patients likely converge upon a common mechanism disrupting the function of this activity switch in telomerase. It is increasingly clear that RNAs have multiple conformations and that proteins can serve to prevent unproductive states or stabilize a preferred state (Schroeder et al., 2004). In this case, telomerase can exist in two alternate conformations and the more highly active conformation is favored by TCAB1 binding.

Several observations support a conformational change for CR4/5 when bound by the TERT TRBD. In a complex with TERT TRBD, the P6.1 stem loop rearranges by more than 180 degrees relative to the CR4/5-only structure (Huang et al., 2014). Thus, the conformation of P6.1 is dramatically altered by protein binding. Taken together, these findings indicate that telomerase can exist in two catalytic states based on altered CR4/5 conformation and that TCAB1 may toggle this RNA activity switch to control telomerase catalytic function.

Convergence of Multiple RNA Domains Working Together in the Holoenzyme

The need for both a template region (PK/T) and an activation domain functionally or structurally analogous to CR4/5 is broadly conserved through evolution of telomerase RNAs (Podlevsky and Chen, 2016). Vertebrate telomerase RNAs also incorporated a third element—the scaRNA domain—not found in telomerase RNAs from single-cell eukaryotes. The scaRNA domain serves a critical role in stabilizing hTR through binding dyskerin, which recognizes the H/ACA motif in hTR. Through binding TCAB1 via the CAB box element, the scaRNA serves a second function in controlling nuclear trafficking of telomerase. Our findings indicate that the TCAB1-CAB box interaction also controls catalytic activity. Once tethered to the CAB box in the scaRNA domain, TCAB1 helps fold P6b and P6.1 into an optimal conformation

for engaging TERT. Alternatively, TCAB1 may facilitate folding of P6b and P6.1 via an allosteric mechanism or by influencing TERT conformation within the complex. Although telomerase RNAs in single-cell organisms lack a scaRNA domain, there are other examples of RNA binding proteins required for telomerase enzyme function. In the single-cell ciliate *Tetrahymena*, p65 protein binds helix IV in telomerase RNA and causes conformational changes in the RNA (Berman et al., 2010). In *S. cerevisiae*, binding of the POP1/6/7 subunits of RNase P/MRP to telomerase RNA is required for enzyme function (Lemieux et al., 2016). Our findings suggest the possibility that the need for a telomerase RNA scaffolding protein may be conserved broadly in evolution, that these telomerase RNA-binding proteins may act in a similar manner as TCAB1 to facilitate folding of key RNA domains, and these functions may be revealed through icSHAPE studies in genetically defined backgrounds analogous to those performed here.

TCAB1 contains a WD40 repeat domain, a molecular scaffold providing diverse surfaces for interactions with proteins and nucleic acids (Castello et al., 2012). For example, the WD40 domain of Germin5 within the SMN complex specifically binds a subset of small nuclear RNAs (snRNAs) (Lau et al., 2009). For TCAB1, the WD40 domain is required for binding the hTR CAB box and may also contact the CR4/5 domain. Through this mechanism, the scaRNA domain influences the activity switch in CR4/5, which in turn works together with PK/T domain to direct telomerase catalytic function. This cooperation between the scaRNA domain and CR4/5 was not readily tested previously because deletion of the scaRNA region abrogates hTR accumulation by eliminating dyskerin binding. A previous study replaced the scaRNA domain in human telomerase with a heterologous 3′ stabilizing RNA element, resulting in an RNP that was catalytically inactive unless TERT was overexpressed (Vogan et al., 2016). Those results indicated a required role for the scaRNA domain in either enzyme assembly or catalytic activation. Our data showing that TCAB1 is needed for folding CR4/5 and for enhancing telomerase catalytic function provide a potential explanation for the lack of telomerase activity seen in cells expressing chimeric telomerase RNA and endogenous TERT. Thus, the scaRNA domain serves both to enable hTR stability and to direct optimal folding of the CR4/5 domain through the action of TCAB1 tethered to the CAB box. In this manner, the scaRNA domain supports the function of CR4/5, which in turn is required for the catalytic cycle involving the PK/T domain.

Trafficking, Recruitment, and Catalysis: TCAB1 Is Required for Several Steps in the Telomerase Pathway

Loss of TCAB1 abrogates telomerase localization within Cajal bodies and diminishes recruitment to telomeres. Our data here showing impaired catalytic function and unfolding of CR4/5 represent a third defect in the telomerase pathway evident in cells lacking TCAB1. It is striking that TCAB1 loss disrupts three seemingly discrete steps in the telomerase pathway: Cajal body localization, telomere recruitment, and CR4/5 folding. TCAB1 serves as the primary recruiter of telomerase and scaRNAs to Cajal bodies, but localization of telomerase to fully formed coilin-positive Cajal bodies is not required for telomerase function, at least in cancer cells where telomerase levels are relatively elevated compared to some primary cell populations. It is possible that, in the absence of coilin, TCAB1 functions in smaller bodies that have thus far eluded detection. We propose that in cells lacking TCAB1 CR4/5 unfolding represents a primary defect that propagates to downstream steps in telomerase function. With CR4/5 partially unfolded and association with the TERT TRBD impaired, catalysis is markedly reduced. Disruption of the CR4/5-TERT TRBD interaction may also explain the diminished recruitment to telomeres in cells lacking TCAB1. Recruitment of telomerase to telomeres depends upon the interaction between the TERT TEN domain and the TEL patch on TPP1. One possibility is that the altered arrangement of CR4/5 and the TERT TRBD may influence the TEN domain in a manner that impairs recruitment to telomeres.

In cells lacking TCAB1, telomeres show profound shortening but apparent stabilization at a very short telomere length. This observation indicates that telomerase with unfolded CR4/5 lacks sufficient activity to maintain bulk telomere length but retains the ability to sustain short telomeres at least in the context of cancer cells or ESCs that express high endogenous levels of TERT. Patients with biallelic mutations in TCAB1 show very short telomeres in blood and develop features of dyskeratosis congenita that are indistinguishable from other severe forms of the disease (Zhong et al., 2011). These observations in patients indicate that important cell populations *in vivo*, such as in blood and epithelial tissues, cannot be maintained in a setting of impaired TCAB1 function. One potential explanation for how tissues fail in TCAB1 mutant patients may relate to lower levels of TERT protein in certain somatic tissues, further compromising telomerase levels (Pech et al., 2015). We propose that the regional unfolding of CR4/5 represents a primary defect in telomerase lacking TCAB1 and that impaired catalysis and diminished recruitment explain the marked telomere shortening that ensues. Taken together, these findings provide evidence for an activity switch in telomerase RNA governed by TCAB1 and controlling telomerase catalytic function. These findings reveal intramolecular conformational changes in the telomerase holoenzyme and suggest novel approaches for interfering with telomerase function in cancer.

STAR★METHODS

Detailed methods are provided in the online version of this paper and include the following:

- KEY RESOURCES TABLE
- CONTACT FOR REAGENT AND RESOURCE SHARING
- EXPERIMENTAL MODEL AND SUBJECT DETAILS
  - Tissue culture cell lines
  - Recombinant protein
- METHOD DETAILS
  - Immunofluorescence staining (IF) and RNA fluorescence *in situ* hybridization (FISH)
  - Telomere Restriction Fragment Analysis (TRF)
  - CRISPR-KO cell line (HeLa)
  - CRISPR-KO cell line (hESCs)
  - Tcab1 flox/null MEFs
  - TRAP (Telomeric Repeat Amplification Protocol)
  - Direct telomerase primer extension assay

- Direct telomerase primer extension assay quantitation
- Immunopurification of endogenous telomerase RNPs
- icSHAPE analysis of telomerase RNPs
- icSHAPE data modeling
- Purification of HA-TCAB1

- QUANTIFICATION AND STATISTICAL ANALYSIS
- DATA AND SOFTWARE AVAILABILITY

SUPPLEMENTAL INFORMATION

Supplemental Information includes seven figures and can be found with this article online at https://doi.org/10.1016/j.cell.2018.04.039.

ACKNOWLEDGMENTS

We are grateful to members of the Artandi laboratory and to D. Herschlag for critical comments. This work was supported by NIH grants CA197563 and AG056575 (S.E.A.), GM122579 and GM102519 (R.D.), and HG004361 (H.Y.C.). C.M.R. was supported by MSTP Training Grant GM007365 and by a Gerald J. Lieberman Fellowship. L.C. was supported by a Stanford Cancer Institute 2018 Fellowship Award.

AUTHOR CONTRIBUTIONS

L.C., A.F., and S.E.A. conceived the study. L.C., C.M.R., A.F., P.J.B., S.T., Y.A.Y., C.R.G., S.L., B.L., M.F.P., and A.S.V. conducted the experiments. L.C., R.D., H.Y.C., and S.E.A. designed the experiments. L.C. and S.E.A. analyzed the data and wrote the paper.

DECLARATION OF INTERESTS

The authors declare no competing interests.

Received: December 21, 2017
Revised: March 22, 2018
Accepted: April 27, 2018
Published: May 24, 2018

REFERENCES

Abreu, E., Aritonovska, E., Reichenbach, P., Cristofari, G., Culp, B., Terns, R.M., Lingner, J., and Terns, M.P. (2010). TIN2-tethered TPP1 recruits human telomerase to telomeres in vivo. Mol. Cell. Biol. *30*, 2971–2982.

Armanios, M., and Blackburn, E.H. (2012). The telomere syndromes. Nat. Rev. Genet. *13*, 693–704.

Batista, L.F., Pech, M.F., Zhong, F.L., Nguyen, H.N., Xie, K.T., Zaug, A.J., Crary, S.M., Choi, J., Sebastiano, V., Cherry, A., et al. (2011). Telomere shortening and loss of self-renewal in dyskeratosis congenita induced pluripotent stem cells. Nature *474*, 399–402.

Berman, A.J., Gooding, A.R., and Cech, T.R. (2010). Tetrahymena telomerase protein p65 induces conformational changes throughout telomerase RNA (TER) and rescues telomerase reverse transcriptase and TER assembly mutants. Mol. Cell. Biol. *30*, 4965–4976.

Cash, D.D., and Feigon, J. (2017). Structure and folding of the Tetrahymena telomerase RNA pseudoknot. Nucleic Acids Res. *45*, 482–495.

Castello, A., Fischer, B., Eichelbaum, K., Horos, R., Beckmann, B.M., Strein, C., Davey, N.E., Humphreys, D.T., Preiss, T., Steinmetz, L.M., et al. (2012). Insights into RNA biology from an atlas of mammalian mRNA-binding proteins. Cell *149*, 1393–1406.

Chen, J.L., Opperman, K.K., and Greider, C.W. (2002). A critical stem-loop structure in the CR4-CR5 domain of mammalian telomerase RNA. Nucleic Acids Res. *30*, 592–597.

Chen, Y., Deng, Z., Jiang, S., Hu, Q., Liu, H., Songyang, Z., Ma, W., Chen, S., and Zhao, Y. (2015). Human cells lacking coilin and Cajal bodies are proficient in telomerase assembly, trafficking and telomere maintenance. Nucleic Acids Res. *43*, 385–395.

Chen, Y., Podlevsky, J.D., Logeswaran, D., and Chen, J.J. (2018). A single nucleotide incorporation step limits human telomerase repeat addition activity. EMBO J. Published online March 15, 2018. https://doi.org/10.15252/embj.201797953.

Cristofari, G., Adolf, E., Reichenbach, P., Sikora, K., Terns, R.M., Terns, M.P., and Lingner, J. (2007). Human telomerase RNA accumulation in Cajal bodies facilitates telomerase recruitment to telomeres and telomere elongation. Mol. Cell *27*, 882–889.

Edgar, R., Domrachev, M., and Lash, A.E. (2002). Gene Expression Omnibus: NCBI gene expression and hybridization array data repository. Nucleic Acids Res. *30*, 207–210.

Flynn, R.A., Zhang, Q.C., Spitale, R.C., Lee, B., Mumbach, M.R., and Chang, H.Y. (2016). Transcriptome-wide interrogation of RNA secondary structure in living cells with icSHAPE. Nat. Protoc. *11*, 273–290.

Folco, E.G., Lei, H., Hsu, J.L., and Reed, R. (2012). Small-scale nuclear extracts forfunctional assays of gene-expression machineries. J Vis Exp. https://doi.org/10.3791/4140.

Freund, A., Zhong, F.L., Venteicher, A.S., Meng, Z., Veenstra, T.D., Frydman, J., and Artandi, S.E. (2014). Proteostatic control of telomerase function through TRiC-mediated folding of TCAB1. Cell *159*, 1389–1403.

Horn, S., Figl, A., Rachakonda, P.S., Fischer, C., Sucker, A., Gast, A., Kadel, S., Moll, I., Nagore, E., Hemminki, K., et al. (2013). TERT promoter mutations in familial and sporadic melanoma. Science *339*, 959–961.

Huang, F.W., Hodis, E., Xu, M.J., Kryukov, G.V., Chin, L., and Garraway, L.A. (2013). Highly recurrent TERT promoter mutations in human melanoma. Science *339*, 957–959.

Huang, J., Brown, A.F., Wu, J., Xue, J., Bley, C.J., Rand, D.P., Wu, L., Zhang, R., Chen, J.J., and Lei, M. (2014). Structural basis for protein-RNA recognition in telomerase. Nat. Struct. Mol. Biol. *21*, 507–512.

Jády, B.E., Bertrand, E., and Kiss, T. (2004). Human telomerase RNA and box H/ACA scaRNAs share a common Cajal body-specific localization signal. J. Cell Biol. *164*, 647–652.

Killela, P.J., Reitman, Z.J., Jiao, Y., Bettegowda, C., Agrawal, N., Diaz, L.A., Jr., Friedman, A.H., Friedman, H., Gallia, G.L., Giovanella, B.C., et al. (2013). TERT promoter mutations occur frequently in gliomas and a subset of tumors derived from cells with low rates of self-renewal. Proc. Natl. Acad. Sci. USA *110*, 6021–6026.

Kim, N.K., Zhang, Q., and Feigon, J. (2014). Structure and sequence elements of the CR4/5 domain of medaka telomerase RNA important for telomerase function. Nucleic Acids Res. *42*, 3395–3408.

Kim, N.W., and Wu, F. (1997). Advances in quantification and characterization of telomerase activity by the telomeric repeat amplification protocol (TRAP). Nucleic Acids Res. *25*, 2595–2597.

Lau, C.K., Bachorik, J.L., and Dreyfuss, G. (2009). Gemin5-snRNA interaction reveals an RNA binding function for WD repeat domains. Nat. Struct. Mol. Biol. *16*, 486–491.

Leeper, T.C., and Varani, G. (2005). The structure of an enzyme-activating fragment of human telomerase RNA. RNA *11*, 394–403.

Lemieux, B., Laterreur, N., Perederina, A., Noël, J.F., Dubois, M.L., Krasilnikov, A.S., and Wellinger, R.J. (2016). Active yeast telomerase shares subunits with ribonucleoproteins RNase P and RNase MRP. Cell *165*, 1171–1181.

Mitchell, J.R., and Collins, K. (2000). Human telomerase activation requires two independent interactions between telomerase RNA and telomerase reverse transcriptase. Mol. Cell *6*, 361–371.

Mitchell, J.R., Wood, E., and Collins, K. (1999). A telomerase component is defective in the human disease dyskeratosis congenita. Nature *402*, 551–555.

Mochizuki, Y., He, J., Kulkarni, S., Bessler, M., and Mason, P.J. (2004). Mouse dyskerin mutations affect accumulation of telomerase RNA and small nucleolar RNA, telomerase activity, and ribosomal RNA processing. Proc. Natl. Acad. Sci. USA *101*, 10756–10761.

Nandakumar, J., Bell, C.F., Weidenfeld, I., Zaug, A.J., Leinwand, L.A., and Cech, T.R. (2012). The TEL patch of telomere protein TPP1 mediates telomerase recruitment and processivity. Nature *492*, 285–289.

Pech, M.F., Garbuzov, A., Hasegawa, K., Sukhwani, M., Zhang, R.J., Benayoun, B.A., Brockman, S.A., Lin, S., Brunet, A., Orwig, K.E., and Artandi, S.E. (2015). High telomerase is a hallmark of undifferentiated spermatogonia and is required for maintenance of male germline stem cells. Genes Dev. *29*, 2420–2434.

Pfeiffer, V., and Lingner, J. (2013). Replication of telomeres and the regulation of telomerase. Cold Spring Harb. Perspect. Biol. *5*, a010405.

Podlevsky, J.D., and Chen, J.J. (2016). Evolutionary perspectives of telomerase RNA structure and function. RNA Biol. *13*, 720–732.

Podlevsky, J.D., Bley, C.J., Omana, R.V., Qi, X., and Chen, J.J. (2008). The telomerase database. Nucleic Acids Res. *36*, D339–D343.

Ran, F.A., Hsu, P.D., Wright, J., Agarwala, V., Scott, D.A., and Zhang, F. (2013). Genome engineering using the CRISPR-Cas9 system. Nat. Protoc *8*, 2281–2308.

Robart, A.R., and Collins, K. (2010). Investigation of human telomerase holoenzyme assembly, activity, and processivity using disease-linked subunit variants. J. Biol. Chem. *285*, 4375–4386.

Schmidt, J.C., and Cech, T.R. (2015). Human telomerase: Biogenesis, trafficking, recruitment, and activation. Genes Dev. *29*, 1095–1105.

Schmidt, J.C., Zaug, A.J., and Cech, T.R. (2016). Live cell imaging reveals the dynamics of telomerase recruitment to telomeres. Cell *166*, 1188–1197.

Schroeder, R., Barta, A., and Semrad, K. (2004). Strategies for RNA folding and assembly. Nat. Rev. Mol. Cell Biol. *5*, 908–919.

Sexton, A.N., Regalado, S.G., Lai, C.S., Cost, G.J., O'Neil, C.M., Urnov, F.D., Gregory, P.D., Jaenisch, R., Collins, K., and Hockemeyer, D. (2014). Genetic and molecular identification of three human TPP1 functions in telomerase action: Recruitment, activation, and homeostasis set point regulation. Genes Dev. *28*, 1885–1899.

Stern, J.L., Zyner, K.G., Pickett, H.A., Cohen, S.B., and Bryan, T.M. (2012). Telomerase recruitment requires both TCAB1 and Cajal bodies independently. Mol. Cell. Biol. *32*, 2384–2395.

Tucker, K.E., Berciano, M.T., Jacobs, E.Y., LePage, D.F., Shpargel, K.B., Rossire, J.J., Chan, E.K., Lafarga, M., Conlon, R.A., and Matera, A.G. (2001). Residual Cajal bodies in coilin knockout mice fail to recruit Sm snRNPs and SMN, the spinal muscular atrophy gene product. J. Cell Biol. *154*, 293–307.

Tycowski, K.T., Shu, M.D., Kukoyi, A., and Steitz, J.A. (2009). A conserved WD40 protein binds the Cajal body localization signal of scaRNP particles. Mol. Cell *34*, 47–57.

Venteicher, A.S., Meng, Z., Mason, P.J., Veenstra, T.D., and Artandi, S.E. (2008). Identification of ATPases pontin and reptin as telomerase components essential for holoenzyme assembly. Cell *132*, 945–957.

Venteicher, A.S., Abreu, E.B., Meng, Z., McCann, K.E., Terns, R.M., Veenstra, T.D., Terns, M.P., and Artandi, S.E. (2009). A human telomerase holoenzyme protein required for Cajal body localization and telomere synthesis. Science *323*, 644–648.

Vogan, J.M., Zhang, X., Youmans, D.T., Regalado, S.G., Johnson, J.Z., Hockemeyer, D., and Collins, K. (2016). Minimized human telomerase maintains telomeres and resolves endogenous roles of H/ACA proteins, TCAB1, and Cajal bodies. eLife. Published online August 15, 2016. https://doi.org/10.7554/eLife.1822.

Vulliamy, T.J., Kirwan, M.J., Beswick, R., Hossain, U., Baqai, C., Ratcliffe, A., Marsh, J., Walne, A., and Dokal, I. (2011). Differences in disease severity but similar telomere lengths in genetic subgroups of patients with telomerase and shelterin mutations. PLoS ONE *6*, e24383.

Wang, F., Podell, E.R., Zaug, A.J., Yang, Y., Baciu, P., Cech, T.R., and Lei, M. (2007). The POT1-TPP1 telomere complex is a telomerase processivity factor. Nature *445*, 506–510.

Yamaguchi, H., Baerlocher, G.M., Lansdorp, P.M., Chanock, S.J., Nunez, O., Sloand, E., and Young, N.S. (2003). Mutations of the human telomerase RNA gene (TERC) in aplastic anemia and myelodysplastic syndrome. Blood *102*, 916–918.

Yoon, S., Kim, J., Hum, J., Kim, H., Park, S., Kladwang, W., and Das, R. (2011). HiTRACE: high-throughput robust analysis for capillary electrophoresis. Bioinformatics *27*, 1798–1805.

Zaug, A.J., Crary, S.M., Jesse Fioravanti, M., Campbell, K., and Cech, T.R. (2013). Many disease-associated variants of hTERT retain high telomerase enzymatic activity. Nucleic Acids Res *41*, 8969–8978.

Zhong, F., Savage, S.A., Shkreli, M., Giri, N., Jessop, L., Myers, T., Chen, R., Alter, B.P., and Artandi, S.E. (2011). Disruption of telomerase trafficking by TCAB1 mutation causes dyskeratosis congenita. Genes Dev. *25*, 11–16.

Zhong, F.L., Batista, L.F., Freund, A., Pech, M.F., Venteicher, A.S., and Artandi, S.E. (2012). TPP1 OB-fold domain controls telomere maintenance by recruiting telomerase to chromosome ends. Cell *150*, 481–494.

Zhu, Y., Tomlinson, R.L., Lukowiak, A.A., Terns, R.M., and Terns, M.P. (2004). Telomerase RNA accumulates in Cajal bodies in human cancer cells. Mol. Biol. Cell *15*, 81–90.

STAR★METHODS

KEY RESOURCES TABLE

REAGENT or RESOURCE	SOURCE	IDENTIFIER
Antibodies		
Anti-Coilin mouse monoclonal	Abcam	Cat# AB11822
Anti-human TCAB1 rabbit polyclonal	Venteicher et al., 2008	n/a
Anti-mouse TCAB1 rabbit polyclonal	This paper	n/a
Ani-HA tag mouse monoclonal (clone HA-7)	Sigma	Cat# H9658
Anti-GAPDH mouse monoclonal (clone GA1R)	ThermoFisher	RRID AB_10977387
Anti-GFP rabbit monoclonal	ThermoFisher	RRID AB_2536526
Anti-β-Tublin mouse monoclonal (clone D-10)	Santa Cruz	Cat# SC-5274
Anti-FLAG mouse monoclonal (clone M2)	Sigma	Cat# F1804
Anti-hTERT rabbit polyclonal	Venteicher et al., 2008	n/a
Anti-Reptin rabbit polyclonal	Venteicher et al., 2008	n/a
Anti-Pontin rabbit polyclonal	Venteicher et al., 2008	n/a
Anti-DKC1 rabbit polyclonal	Gift from Dr. Mason Mochizuki et al., 2004	n/a
Bacterial and Virus Strains		
DH5α competent cell	ThermoFisher	Cat# 18265017
OneShot Top10 competent cell	ThermoFisher	Cat# C404050
BL21 (DE3+)	NEB	Cat# C2527I
Adenovirus encoding eGFP	University of Iowa, Viral Vector Core	Cat #: VVC-U of Iowa-4
Adenovirus encoding Cre-eGFP	University of Iowa, Viral Vector Core	Cat #: VVC-U of Iowa-1174
Chemicals, Peptides, and Recombinant Proteins		
3xHA peptide	Sigma	Cat# I-2149
MBP/GST tagged mouse TCAB1	This study	n/a
3xHA tagged human TCAB1	This study	n/a
Deposited Data		
The icSHAPE data	This study	GSE97486
Raw data and relevant analysis for constructing figures	Mendeley Data	https://doi.org/10.17632/3tsfhxtmys.1
Experimental Models: Cell Lines		
HeLa S3	ATCC	Cat# CCL-2.2
HEK293T	ATCC	Cat# CRL-11268
Tcab1 flox/null MEFs	This study	n/a
human WA01 H1 hESC (male origin)	WiCell	Cat# NIHhESC-10-0043/WB16218
Oligonucleotides		
Guide RNA oligo (FWD) for TCAB1 CRISPR	CACCGGGCGGATCCCCCCTTTCGGG	n/a
Guide RNA oligo (REV) for TCAB1 CRISPR	AAACCCCGAAAGGGGGGATCCGCCC	n/a
Guide RNA oligo (FWD) for Coilin CRISPR	CACCGAAGCCGTAGCCTAACCGTCT	n/a
Guide RNA oligo (REV) for Coilin CRISPR	AAACAGACGGTTAGGCTACGGCTTC	n/a
hTR FISH probes	GCCCTTCTCAGTTAGGGTTA; AAGTCAGCGAGAAAAACAGC; TCTAGAATGAACGGTGGAAG; CCAGCAGCTGACATTTTTTG; GCTGACAGAGCCCAACTCTT; GTCCCACAGCTCAGGGAATC; CATGTGTGAGCCGAGTCCTG	n/a

(*Continued on next page*)

Continued

REAGENT or RESOURCE	SOURCE	IDENTIFIER
^{32}P End labeled oligonucleotide probe for TRF	CCCTAACCCTAACCCTAA	n/a
^{32}P End labeled TS primer for TRAP	AATCCGTCGAGCAGAGTT	n/a
Primer a5 for direct telomerase assay	TTAGGGTTAGGGTTAGCGTTA	Wang et al., 2007
Recombinant DNA		
pSpCas9(BB)-2A-GFP (px458)	A gift from Feng Zhang	Addgene plasmid # 48138
pMGIB HA-TCAB1	This study	n/a
pBluescript-U1-hTR and its derivatives	This study	n/a
pcDNA-3xFLAG-hTERT	This study	n/a
Software and Algorithms		
GraphPad Prism Software	GraphPad software	https://www.graphpad.com/scientific-software/prism/
TotalLab Quant software	TotalLab Ltd	http://totallab.com/
HiTRACE software package version 2.0	Yoon et al., 2011	http://hitrace.org/index.php/page/view/about
Other		
Telomerase database for secondary structure and disease mutations	Podlevsky et al., 2007	http://telomerase.asu.edu/
Protocol for direct telomerase primer extension assay	Zaug et al., 2013	https://www.colorado.edu/lab/cech/lab-protocols

CONTACT FOR REAGENT AND RESOURCE SHARING

Further information and requests for resources and reagents should be directed to and will be fulfilled by the Lead Contact, Steven E. Artandi (sartandi@stanford.edu)

EXPERIMENTAL MODEL AND SUBJECT DETAILS

Ethical compliance: All animal protocols were approved by the Institutional Animal Care and Use Committee at Stanford University. All experiments complied with the relevant ethical regulations of Stanford University.

Tissue culture cell lines

- HeLa S3: a subclone of the parental HeLA cell line derived from cervical adenocarcinoma of a female; were cultured in DMEM containing 10% fetal bovine serum at 37°C, 5% CO2; obtained from ATCC (CCL-2.2).
- HEK293T: a highly transfectable subclone of the Human Embryonic Kidney (HEK) epithelium cell line stably expressing SV40 large T antigen; female origin; were cultured in DMEM containing 10% fetal bovine serum at 37°C, 5% CO_2; obtained from ATCC (CRL-11268).
- *Tcab1* flox/null MEFs: were generated from E14.5 mouse embryos and cultured in DMEM containing 10% fetal bovine serum and 1% penicillin/streptomycin at 37°C, 5% CO_2, and 3% O_2. Passage 3 MEFs were infected three times each with 107 PFU of Adenovirus encoding Cre-eGFP or eGFP (University of Iowa, Viral Vector Core).
- Human Embryonic Stem Cell (hESC): Passage 29 human WA01 H1 hESC (male origin) were grown in mTeSR1 (Stem Cell #05850) feeder free system on matrigel (Corning 356230) coated plates at 37°C, 5% CO_2; obtained from WiCell (NIHhESC-10-0043/WB16218)

Recombinant protein

- Recombinant mouse TCAB1 for antibody production: *E. coli.* BL21 (DE3) were transformed with bacterial expression vector encoding mouse TCAB1 cDNA fused with N-terminal epitope tags (GST or MBP). Colonal cells were isolated and expanded in LB medium containing 0.2% glucose and 100 μg/ml Ampicillin. Cells were cultured in a shaker at 250 rpm, 37°C until OD reached 0.6. Recombinant protein expression was induced by adding 0.3M of IPTG at 32°C for 5 hours. Cells were harvested by centrifuging at 4°C, 4000x g for 20min.

- Recombinant human TCAB1 for biochemical reconstitution: HeLa S3 (female origin) were grown as suspension culture in 2L Square bottles (Nalgene square PETG) with constant agitation (rotation radius < 1 inch) at 37°C, 5% CO_2 in Serum-free Freestyle medium (ThermoFisher 12338018) at a density below $1x10^6$ per ml.

METHOD DETAILS

Immunofluorescence staining (IF) and RNA fluorescence *in situ* hybridization (FISH)

All immunofluorescence was carried out on cells seeded on coverslips. Cells were fixed with 10% formalin and permeabilized with 0.1% Triton X-100 in PBS. Coverslips were incubated with primary antibody to coilin (Abcam, AB11822) and/or primary antibody to TCAB1 (Venteicher et al., 2009) in 1% BSA for 1 hr at room temperature. Coverslips were washed 3x with PBS and incubated with secondary Alexa Flour conjugated antibodies (Jackson Immunoresearch) in 1% BSA for 45 minutes at room temperature. Coverslips were washed 3x in PBS and then dehydrated for 10 min in 70% ethanol in preparation for RNA FISH. RNA FISH was done using labeled oligonucleotide probes (Biosearch). Ethanol was removed and RNA FISH probes (Biosearch Technologies, Quasar 570 conjugated, 75 nM working concentration) in RNA FISH hybridization buffer (2x SSC, 10% Formamide, and 10% dextran sulfate) was immediately added. Coverslips were incubated at 37°C overnight, then washed twice with 2x SSC, 10% Formamide at 37°C for 30 min each. Coverslips were mounted in 2x SSC. For each genotype, > 50 nuclei were scored for the number of hTR foci at telomeres. Error bars, S.E.M, and significance were calculated by Student's t test in GraphPad Prism Software.

Telomere Restriction Fragment Analysis (TRF)

To measure telomere lengths, ~$1x10^6$ cells were harvested and digested overnight in tail lysis buffer (100nM Tris-HCl, pH = 8.5, 5mM EDTA, 200mM NaCl, 0.2% SDS, and Proteinase K at 60 μg/mL) at 55°C. DNA was extracted by the phenol-chloroform method and digested with HinfI and RsaI for 20 hours at 37°C. 3 μg of digested DNA was loaded onto a 0.8% agarose gel (1x TBE), and separated by electrophoresis at 85 V for 16 hours at room temperature. DNA was transferred to Hybond N membrane by upward capillary action, and crosslinked to the membrane in an UV crosslinker (Stratalinker 1800). Standard Southern blotting procedure was carried out to detect telomeric restriction fragments using $(CCCTAA)_4$ oligonucleotide probe end-labeled with radio-isotope ^{32}P.

CRISPR-KO cell line (HeLa)

HeLa S3 and 293T cells were cultured in DMEM containing 10% fetal bovine serum at 37°C, 5% CO_2. Lipofectamine 2000 (Life Technologies) was used for all cDNA transfection experiments. TCAB1-KO cells were generated by transfection of HeLa cells with pSpCas9-2A-GFP (PX458) (Ran et al., 2013) plasmid encoding 3x FLAG Cas9-T2A-GFP and guide RNAs to the TCAB1 and Coilin locus. Sequences of guide RNAs are as follows: TCAB: GCGGATCCCCCCTTTCGGG; Coilin: AAGCCGTAGCCTAACCGTCT. GFP-positive cells were single-cell cloned into 96 well plates by FACS and clones were screened for knock-out by IF and immunoblotting using anti-human TCAB1 polyclonal antibody. To generate stable HA-TCAB1-expressing rescuing cells, 293T cells were transfected with pMGIB HA-TCAB1 and packaging constructs; 48 hours later, viral supernatant was collected and concentrated using Retro-X (Clontech). HeLa TCAB1-KO clones were transduced in the presence of 5 μg/ml polybrene and selected in 10 μg/mL blasticidin for 5-7 days.

CRISPR-KO cell line (hESCs)

Passage 29 human WA01 H1 hESC were grown in mTeSR1 (Stem Cell #05850) feeder free system on matrigel (Corning 356230) coated plates. For transfection, cells were incubated with Thiazovivin (Santa cruz sc-361380) at 2 uM for 1 hour. Cells were treated with Accutase to single cell suspension and then pelleted and resuspended in DNA/lipofectamine solution and incubated at RT for 10-15 minutes. Cells were replated in thiazovivin-containing media on matrigel. At 48 hours post-transfection, cells were FACs sorted based on GFP expression and selected colonies were expanded for screening by immunoblotting.

Tcab1 flox/null MEFs

TCAB1 delta/flox and TCAB1 wt/wt MEFs were generated from E14.5 embryos and cultured in DMEM containing 10% fetal bovine serum and 1% penicillin/streptomycin at 37°C, 5% CO_2, and 3% O_2. Passage 3 MEFs were infected three times each with $1x10^7$ PFU of Adenovirus encoding Cre-eGFP or eGFP (University of Iowa, Viral Vector Core). Anti-mouse TCAB1 polyclonal antibody was generated by injecting MBP tagged recombinant mouse TCAB1 protein into rabbits for anti-serum production. The antibody was purified by affinity chromatography. Briefly, GST tagged mouse TCAB1 protein was crosslinked to glutathione column using disuccinimidyl suberate (DSS). Anti-mouse TCAB1 antibody that bound to the affinity column was eluted by 0.1M Glycin-HCl pH 2.0.

TRAP (Telomeric Repeat Amplification Protocol)

To measure telomerase activity, a two-step TRAP procedure was performed according to (Kim and Wu, 1997). Briefly, cell extracts or protein fractions were incubated with telomeric primers for a 30 min initial extension step at 30°C in a PCR machine, followed by 5 min of inactivation at 72°C. Without purification, 1 μl of the extended reaction was subjected to PCR amplification (24 cycle of 30 s at 94°C, followed by 30 s at 59°C) in presence of ^{32}P end-labeled telomeric primers that has been purified using a micro-spin

G-25 column (GE healthcare, 27-5325-01). The PCR reactions were resolved by 9% polyacrylamide gel electrophoresis at room temperature, and the gel was exposed to a phosphor-imager and scanned by a Typhoon scanner. The scanned image was quantitated using the TotalLab Quant software. Multiple biological replicates (independently derived cell clones, or MEF lines derived from different animals) were included in each assay. Representative gel images were presented among at least 3 repeats.

Direct telomerase primer extension assay

Direct telomerase assay was performed essentially as in https://www.colorado.edu/lab/cech/lab-protocols, except a few modifications. The 20μl reaction mixture contains 50mM NaCl instead of KCl, and was incubated at 30°C for 2 hours. The reaction mixture was extracted by phenol-chloroform prior to ethanol precipitation. The aqueous phase separation was assisted by using phase-lock gel. In addition, the 75% ethanol washing solution residing with the final DNA pellet was thoroughly removed by pipetting with a loading tip, instead of speed vacuuming. The sequencing gel was also fixated in 10% methanol and 10% glacial acetic acid (v/v) solution for 30 minute prior to gel drying. 10 bp DNA ladder (ThermoFisher 10821015) was end-labeled using T4 polynucleotide kinase (PNK). Multiple biological replicates (independently derived cell clones) were included in each assay. Representative gel images were presented among at least 3 repeats.

Direct telomerase primer extension assay quantitation

To calculate the overall specific activity as the incorporation rate of ^{32}P-GMP into elongating telomere substrates per RNP, the intensity of the extended primer (a5+GGG) and each of the principal extension products (+9, +15, etc) were quantified. The products that are not readily resolved by the gel were not counted. The collective radio-density of telomeric bands in each lane was then normalized to the corresponding recovery control (RC), which is an end-labeled spike-in TS primer during the DNA purification procedure. To calculate the processivity (repeat addition processivity, RAP) of telomerase RNPs, radio-density for each telomerase-extended species is normalized by the predicted number of ^{32}P-GMP incorporated (value in Log_{10}), and plotted versus the actual repeat number. Telomerase processivity measures the number of repeats synthesized before half of the chains have dissociated ($R_{1/2}$), following the equation:

$$R_{1/2} = \frac{-\ln 2}{2.303k}$$

The slope k was extrapolated based on the graph.

Immunopurification of endogenous telomerase RNPs

Rabbit polyclonal anti-TERT antibody (T421) used to purify endogenous telomerase RNPs from various cell lines were generated by immunizing rabbits with recombinant TERT fragment 421-493 fused with a MBP tag. Anti-TERT antibody was then affinity purified by pull down using GST tagged TERT 421-493, and characterized extensively in Venteicher et al., 2008 and in Figure S4A. Nuclear extracts were prepared from indicated HeLa cells per Folco et al., 2012. Typically, 30 μg of T421 antibody was incubated with 1ml of nuclear extract prior to addition of protein A-agarose Fast Flow (P3476 Sigma). Immunoprecipitated complex was washed extensively with Lys450 (20 mM HEPES-NaOH pH7.9, 450 mM NaCl, 0.5% Triton X-100, 10 mM KCl, 4 mM $MgCl_2$, 0.2mM EDTA, 10% Glycerol, freshly add 1 mM DTT, 200 μM PMSF, and Protease Inhibitor Cocktail [P8340 Sigma]), then equilibrated as a 50% slurry in 1x direct assay buffer (50 mM Tris-HCl pH 8.0, 50 mM KCl, 1 mM MgCl2, 1 mM Spermidine, 5 mM β-mercaptoethanol, and 30% Glycerol), lastly aliquoted and snap-froze on dry ice and store in −80°C freezer. Fresh aliquots were used in western and Northern blottings, telomerase assays, and icSHAPE analysis.

icSHAPE analysis of telomerase RNPs

SHAPE modifier NAI-N_3 were used to interrogate the RNA structure at single nucleotide resolution by preferentially acylating flexible residues. Purified telomerase RNP were thawed on ice and equilibrated at 37°C for 30 min. NAI-N_3 was added to a final concentration of 100 μM and incubated for 12 min. An equal volume of DMSO was added in parallel as mock treated samples. Reaction was stopped by addition of TRIzol LS reagent. Total RNA was recovered and libraries were constructed according to Flynn et al., 2016. Briefly, NAI-N_3 modified RNAs were fragmented to ~100nt and ligated with DIBO-biotin using CLICK-it reactions. The modified RNAs were selectively purified by biotin-mediated pull-down, and subjected to cDNA synthesis by reverse transcription. PCR-amplified cDNA libraries were subjected to Next-Generation sequencing. SHAPE data analysis was performed as described in Flynn et al., 2016. Two technical replicates were analyzed for each sample, including both NAI-N_3 treated and DMSO-treated. Two biological replicates were performed for each telomerase RNPs. Identity of all samples were blinded throughout the pipeline until the final data analysis.

icSHAPE data modeling

Secondary structure diagrams are adapted from Telomerase Database (Podlevsky et al., 2008) and edited using Illustrator (Adobe). The HiTRACE software package version 2.0 (Yoon et al., 2011) was used to color icSHAPE reactivity.

Purification of HA-TCAB1

The procedure was described in Chen et al., 2014. Briefly, Dignam nuclear extract was prepared from HeLa TCAB1-KO clonal cells stably expressing 3x HA epitope tagged TCAB1 cDNA. The cells were growing as suspension culture in serum-free Freestyle medium (ThermoFisher 12338018) using 2L square bottles (Nalgene square PETG). Pre-cleared nuclear extract was split in half, with one half treated with 0.1 μg/ul RNase A (ThermoFisher EN0531). Immunoprecipitated HA agarose (Sigma A2095) was washed extensively with Lys450 buffer. HA-TCAB1 was eluted in EB50 (10 mM HEPES pH 7.9, 10% glycerol, 50 mM NaCl, 1.5 mM MgCl2, 0.05% Triton X-100, and freshly added 1 mM DTT, 200 μM PMSF, and Protease Inhibitor Cocktail) containing 0.25 mg/ml 1xHA peptide. 20x volume of bed volume of eluate was collected, passed through an empty chromatography column (BIO-RAD 7326204), and finally concentrated ~10x by passing through a 10kD MWCO Amicon Ultra Centrifugal Filter Device (UFC 801024).

QUANTIFICATION AND STATISTICAL ANALYSIS

Data analysis and visualization of all gel-based and q-PCR assays were aided by Daniel's XL Toolbox add-in for Excel, version 7.2.12, by Daniel Kraus, Würzburg, Germany (https://www.xltoolbox.net). Error bars presented represent S.D.; *p* values were calculated by Student's t test; $p < 0.05$ was defined as significant. Error bars, S.E.M, and significance of the IF data were calculated by Student's t test in GraphPad Prism Software. Statistical details can be found in figures, and in the Results section. Statistical tests used and exact value of "n" can be found in corresponding "Method Details" sessions.

DATA AND SOFTWARE AVAILABILITY

The icSHAPE data have been deposited in NCBI's Gene Expression Omnibus (Edgar et al., 2002) and are accessible through GEO Series accession number GEO: GSE97486 (https://www.ncbi.nlm.nih.gov/geo/query/acc.cgi?acc=GSE97486).

For Raw data used to construct the Figures, please refer to data depository hosted by Mendeley via the following URL: https://doi.org/10.17632/3tsfhxtmys.1

Parental cell	Clone Name/Allele	Sequence
HeLa	WT TCAB1	41 42 43 44 45 46 47 48 49 50 ATG CCA CCG CCT CCC GAA AGG GGG GAT CCG Met Pro Pro Pro Pro Glu Arg Gly Asp Pro
	TKO-1 A8 (15 clones) Glu46 Arg_fs* Glu46Thr_fs* Pro44*	ATG CCA CCG CCT CCC CGA AAG GGG GGA TCC ATG CCA CCG CCT CCC ACC CGA GTG GAA TGG ATG CCA CCG --T - - - GAA AGG GGG GAT CCG
	TKO-2 C1 (14 clones) Pro43Lys_fs* Glu46Ala_fs* Pro44Lys_fs*	ATG CC- --- --- --- GAA AGG GGG GAT CCG ATG CCA CCG CCT CCC G-- --- - - - CCT CAG ATG CCA CC- --- --- GAA AGG GGG GAT CCG
	TKO-3 D9 (13 clones) Pro42Arg_fs* Glu46Gly_fs*	ATG C-- - -- --- --- --- --- --- --- GAT CCG ATG CCA CCG CCT CCC GGA AAG GGG GGA TCC
	TKO-4 C3 (20 clones) Glu46Gly_fs* Pro45Lys_fs*	ATG CCA CCG CCT CCC --- --- --- G GAT CCG ATG CCA CCG CC - --- GAA AGG GGG GAT CCG
	TKO-5 C5 (14 clones) Pro45Arg_fs* Glu46Lys_fs* Pro42Arg_fs*	ATG CCA CCG CCT C-- GAA AGG GGG GAT CCG ATG CCA CCG CCT CC - GAA AGG GGG GAT CCG ATG C-- --- --- --- GAA AGG GGG GAT CCG
	TKO-6 C9 (29 clones) Glu46Lys_fs* Arg47Gly_fs* Asp37Gly_fs*	ATG CCA CCG CCT CCC --A AGG GGG GAT CCG ATG CCA CCG CCT CCC GAA - GG GGG GAT CCG 34 bp deletion bp 110-143

Parental cell	Clone Name/Allele	Sequence
hESC H1	H1 WT TCAB1	41 42 43 44 45 46 47 48 49 50 ATG CCA CCG CCT CCC GAA AGG GGG GAT CCG Met Pro Pro Pro Pro Glu Arg Gly Asp Pro
	H1 TCAB1 #1 (6 clones) Glu46Lys_fs* Glu46Gly_fs*	ATG CCA CCG CCT CCC AA- --- GGG GGA TCC ATG CCA CCG CCT CCC GGA AAG GGG GGA TCC
	H1 TCAB1 #10 (7 clones) Glu46Gly_fs* Glu46Gly_fs*	ATG CCA CCG CCT CCC GGA AAG GGG GGA TCC ATG CCA CCG CCT CCC G-- --- --- --- --- (19 bp deletion)
	H1 TCAB1 #37 (19 clones) Glu46Ala_fs* Glu46Pro_fs*	ATG CCA CCG CCT CCC G-- --- --- --- --- (14 bp deletion) ATG CCA CCG CCT CCC --- -- - --- --- --- (17 bp deletion)

Parental cell	WT COIL	1 2 3 4 5 6 7 8 9 10 11 12 13 14 ATG GCA GCT TCC GAG ACG GTT AGG CTA CGG CTT CAA TTT GAT Met Ala Ala Ser Glu Thr Val Arg Leu Arg Leu Gln Phe Asp
HeLa	CKO-1 A9 (14 clones) Thr6Ile_fs* Thr6Arg_fs* Ala3Phe_fs*	ATG GCA GCT TCC GA- --- --- --- --- --- --- --- --- --- GAT ATG GCA GCT TCC GAG AGA AAC ACT CTT TTT GTA GTA TCT GGA ATG GCA --T T-- --- --- -TT -G - --A --- -TT CAA TTT GAT
	CKO-4 C3 (10 clones) Thr6Lys_fs*	ATG GCA GCT TCC GAG A-- --- AGG CTA CGG CTT CAA TTT GAT
	CKO-5 C5 (13 clones) Thr6Arg_fs* Thr6Ala_fs* Thr6Ile_fs*	ATG GCA GCT TCC GAG - CG GTT AGG CTA CGG CTT CAA TTT GAT ATG GCA GCT TCC GAG --- --- --G CTA CGG CTT CAA TTT GAT ATG GCA GCT TCC GAG A-- --T AGG CTA CGG CTT CAA TTT GAT
	WT COIL	61 62 63 64 65 66 67 68 69 70 71 72 73 CTG GAG GGG GGG CTC TTG CCC CCC GCC GAG AGC GCG CGC Leu Glu Gly Gly Leu Leu Pro Pro Ala Asp Ser Ala Arg
	CKO-2 E1 (8 clones) Ser71Arg_fs* Pro68Gly_fs*31 Gly63Arg_fs*13 Pro67*	CTG GAG GGG GGG CTC TTG CCC CCC GCC GAG AGG CGC GCG CTG GAG GGG GGG CTC TTG CCT GGT AGT GGA GGG GGA TGG CTG --- --- --- --- --- --- --- --- --- --G AGC GCG CGC CTG GAG GGG GGG CT- --- --- --- --- --- --- --- --- ---
	WT COIL	44 45 46 47 48 49 50 51 52 53 54 55 56 57 CTC ATC CGC CAG CGC TTC GGC TTC AGT TCT GGG GCC TTC CTA Leu Ile Arg Gln Arg Phe Gly Phe Ser Ser Gly Ala Phe Leu
	CKO-3 A12 (16 clones) Arg48Pro_fs* Phe49Gln_fs*	CTC ATC CGC CAG C-C TTC GGC TTC AGT TCT GGG GCC TTC CTA CTC ATC CGC CAG CG- --- --- -TC AGT TCT GGG GCC TTC CTA

(legend on next page)

Figure S1. Genotyping Result of CRISPR/Cas9 Edited Human Cell Clones, Related to Figure 1

Genotyping PCR on genomic DNA harvested from HeLa TCAB1-KO clones (upper table, TKOs), hESC H1 cell clones (middle table), and HeLa Coilin-KO clones (lower table, CKOs). The position of PCR amplicon is indicated. The number of bacterial clones sequenced is shown for each clone. Sequence for all identified alleles were shown in comparison to the WT allele. FS, frameshift mutation. The number of TCAB1 and Coilin alleles recovered by genotyping varies clonally.

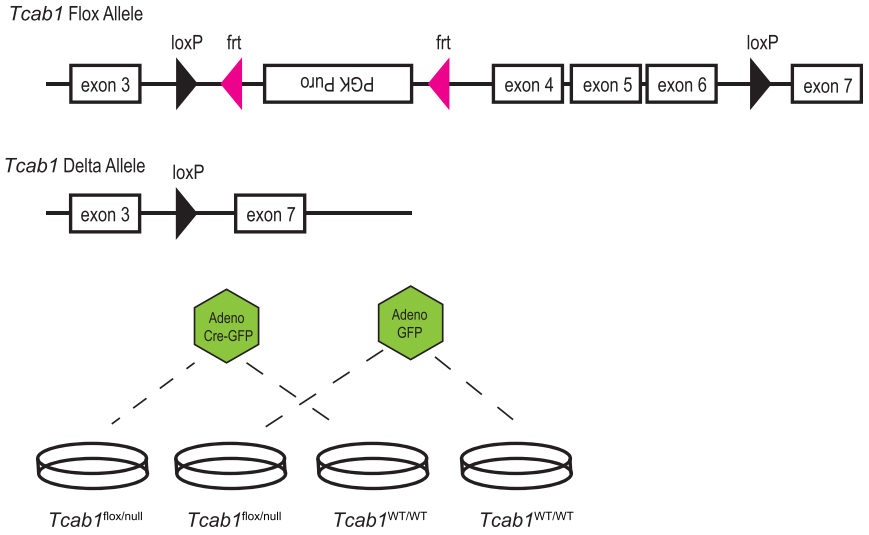

Figure S2. Schematics for Conditional Knockout Tcab1 Allele in MEFs, Related to Figure 1

Allelic structure of mouse Tcab1 gene prior and post to the Cre-mediated recombination at lox P sites (black triangle). Adenovirus encoding either Cre-GFP fusion or GFP alone (Green hexagons) were used to transduce mouse embryonic fibroblasts (MEFs) derived from individual mouse embryos with indicated genotype.

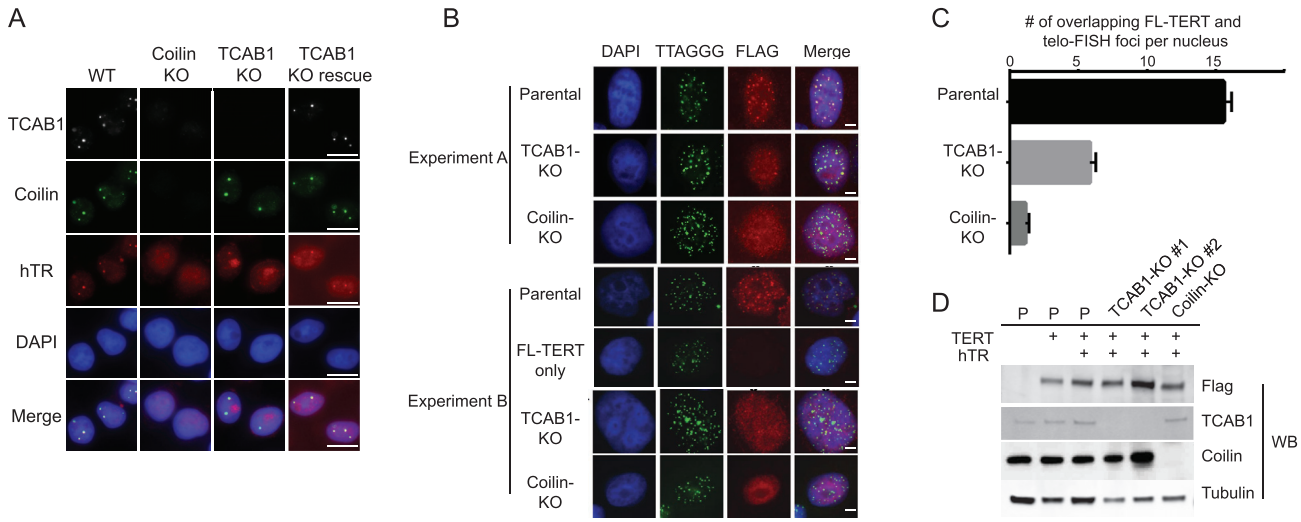

Figure S3. hTR Localization and Telomerase Recruitment in Cells Lacking TCAB1 and Coilin, Related to Figure 2

(A) Cellular localization of hTR (Red), TCAB1 (white), and Coilin (green) in CRISPR/Cas9-derived HeLa cell clones by combined RNA FISH and immunofluorescence. WT, parental HeLa cells; Coilin-KO, coilin KO HeLa cells; TCAB1-KO clone A8; TCAB1-KO rescue, TCAB1-KO clone A8 rescued by stably expressing 3HA-TCAB1. Scale bars, 20 μm source data.

(B) Telomerase recruitment to telomeres, similar as in Figure 2, in parental HeLa and TCAB1 or Coilin KOs transfected with plasmids encoding FLAG-TERT and hTR. Telomere is marked by DNA FISH; FLAG-TERT is detected by IF using anti-FLAG antibody. Two independent experiments are shown. Scale bars, 5 μm source data.

(C) The number of FLAG-TERT foci co-localized with telomeres marked by telo-DNA FISH is quantified. For each genotype, > 70 nuclei were scored for the number of hTR foci at telomeres.

(D) Protein expression in super-telomerase cells assayed by immunoblotting.

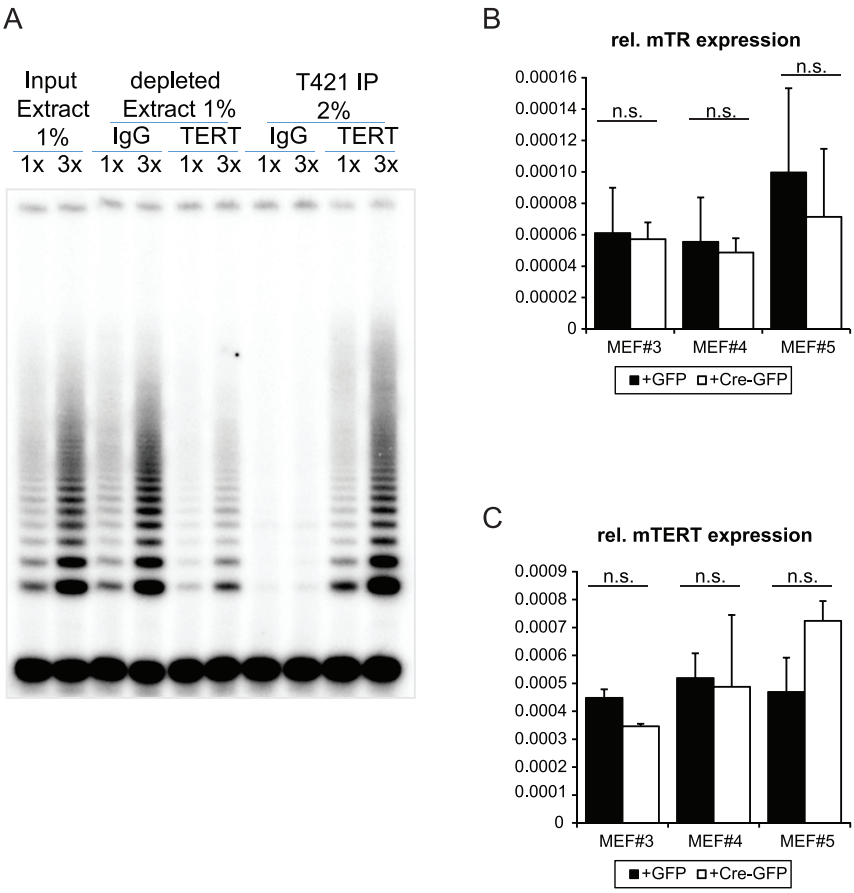

Figure S4. Anti-hTERT Immunoprecipitation and Mouse Telomerase Expression, Related to Figures 1 and 3

(A) anti-hTERT immunoprecipitation quantitatively depletes cellular telomerase activity. Anti-hTERT immunoprecipitation (T421, affinity-purified rabbit polyclonal antibody) was performed using nuclear extract from WT HeLa cells. Shown is the TRAP activity measured from Input and IP-depleted extracts, and the immunoprecipitated fractions. IgG IP as a mock control.

(B and C) Cre-mediated mTCAB1 deletion does not affect the mRNA expression of mTR (B) and mTERT (C). qPCR analysis on total RNA isolated from MEFs (#3,4-TCAB1flox/null, #5-WT,) infected by retrovirus encoding either GFP (black bars) or Cre-GFP fusion (white bars).

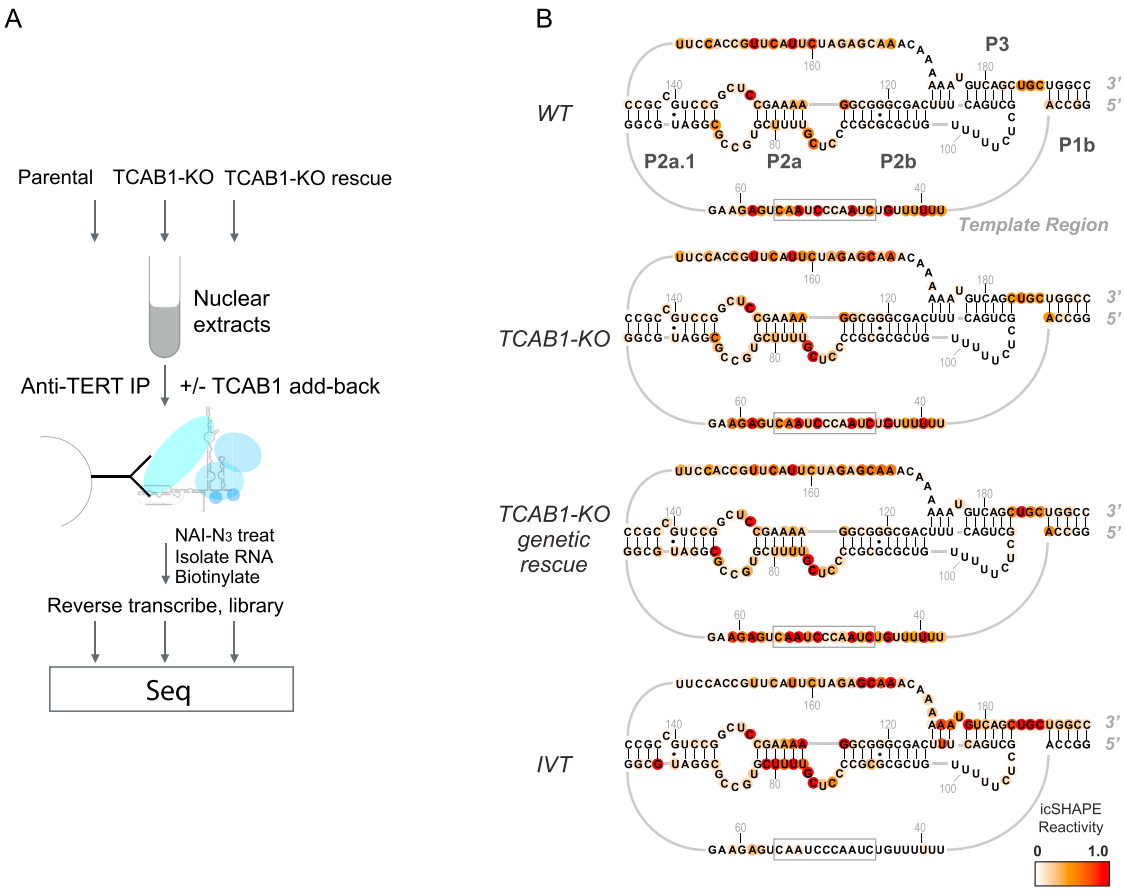

Figure S5. icSHAPE Pipeline and the Reactivity of PK/T Domain of TERT-Bound hTRs, Related to Figure 5

(A) Schematic outline of the icSHAPE pipeline. Telomerase RNPs purified from indicated cell background were treated with icSHAPE modifier NAI-N_3 *in vitro*. Biochemical reconstitution of purified 3HA-TCAB1 was incubated with RNPs before the NAI-N_3. RNA was isolated by Trizol reagent, and biotinylated by "CLICK" chemistry. After the reverse transcription step, biotinylated molecule was isolated. cDNA was eluted and prepared into library before Next-Gen sequencing.

(B) icSHAPE reactivity of pseudoknot/template (PK/T) domain of hTR. Residues within the PK domain of hTR are color-coded according to their icSHAPE reactivity, and modeled onto the secondary structure of hTR obtained from the Telomerase Database. Shown is the data obtained from 3 different telomerase RNPs and the *in vitro* transcribed (IVT) naked hTR (bottom). The template region of hTR is boxed in Grey.

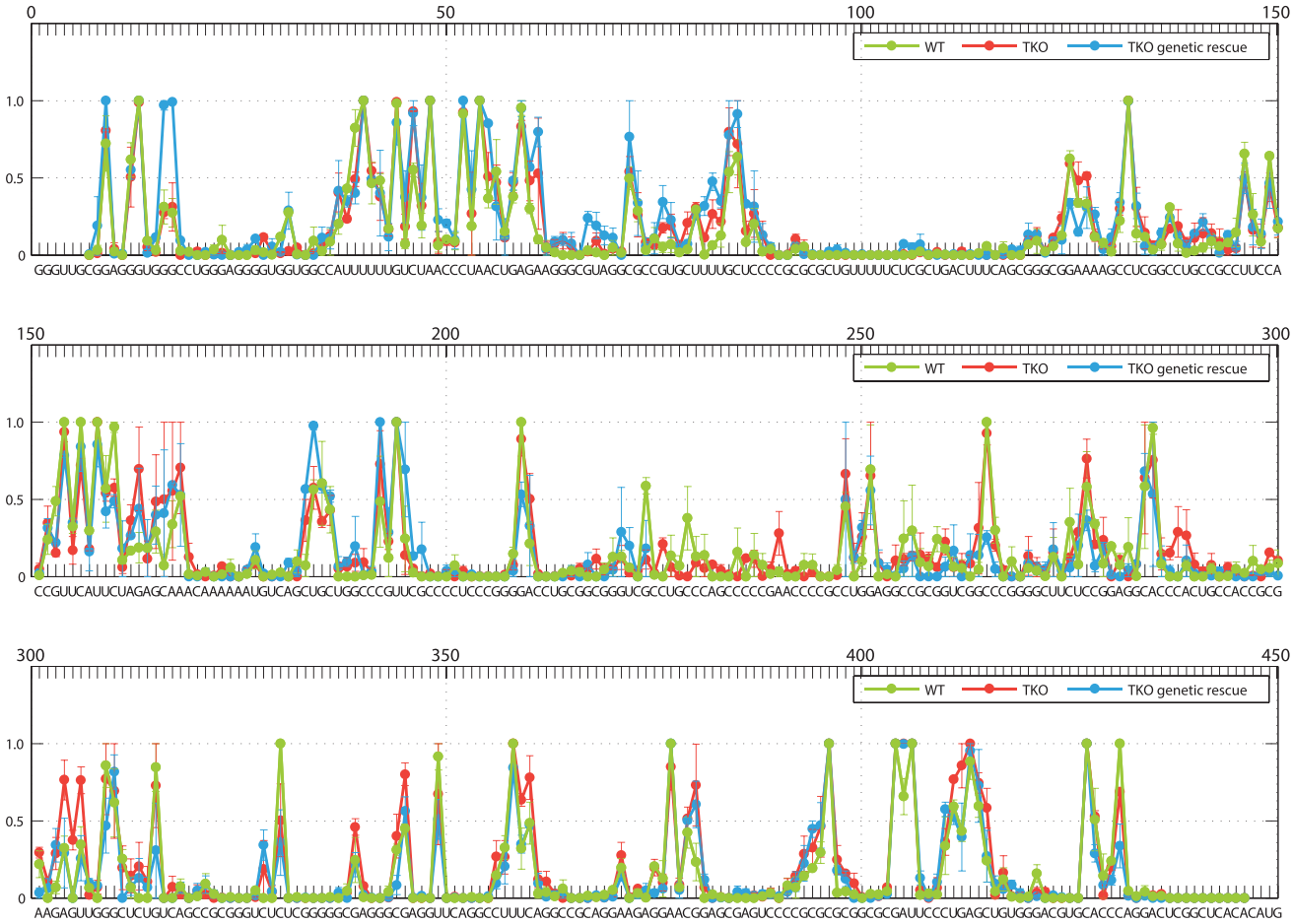

Figure S6. Primary icSHAPE Reactivity of Telomerase RNPs across the Entire hTR Molecule, Related to Figure 5

Nucleotide-specific icSHAPE reactivity of hTR is shown as green track for the WT RNP, Red for the TCAB1-KO RNP, and Blue for RNP purified from TCAB1-KO cells rescued by re-expressing 3HA-TCAB1 cDNA. Error bars are derived from SD of 2 technical replicates.

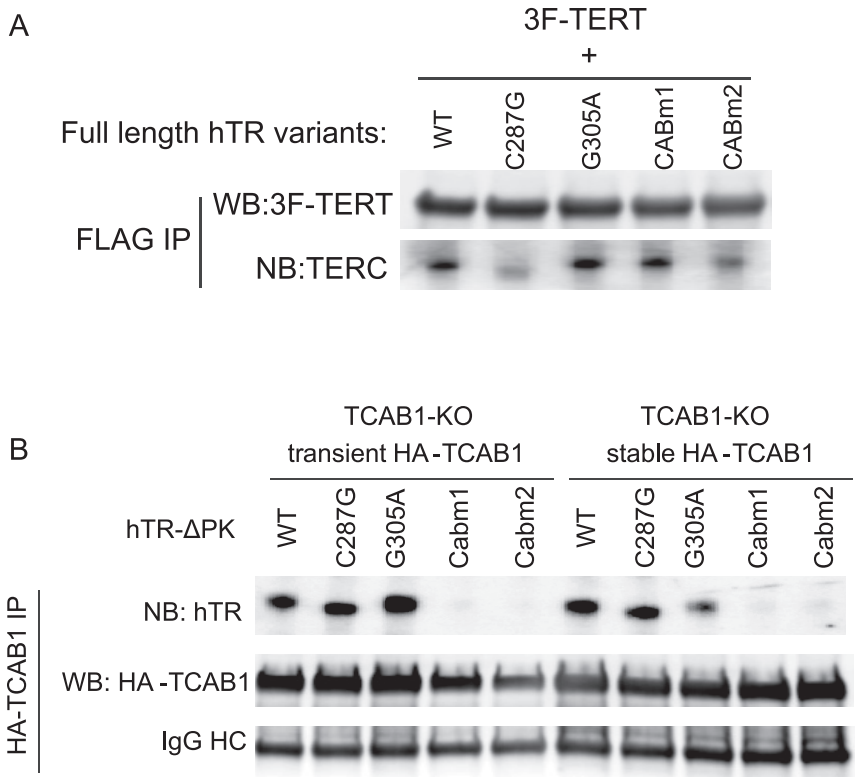

Figure S7. Super-telomerase RNP Quantitation and TCAB1 Association with hTR Variants, Related to Figure 6

(A) Telomerase RNPs containing hTR variants reconstituted in super-telomerase cells. Super-telomerase RNPs were reconstituted in 293T cells by transiently co-expressing 3xFLAG epitope tagged TERT and various full-length hTR variants as indicated. The RNPs were purified by FLAG immunoprecipitation, and characterized by anti-FLAG western blotting and hTR probe in Northern blotting.

(B) CR4/5 mutants retain stable association with TCAB1. HA-TCAB1 expressing HeLa cells were generated by either transiently transfecting TCAB1-KO cells with a TCAB1-expressing plasmid (left) or by lentiviral-mediated stable expression in TCAB1-KO cells (right). hTR-ΔPK (209-451) variants, including C287G, G305A, G414C (CAB box mut1), and G412C (CAB box mut2), were co-expressed by transient transfection. HA-TCAB1 immunoprecipitations were performed from whole cell extracts as mentioned in the method session. Half of the immunoprecipitated fraction were eluted by SDS and analyzed by western blotting for TCAB1. The other half eluted by Trizol and analyzed by Northern blotting using probes generated by random-priming onto full-length hTR.